Numerical evaluation of a non-conforming discontinuous Galerkin method on triangular meshes for solving the time-domain Maxwell equations

Hassan Fahs

INRIA

INSTITUT NATIONAL DE RECHERCHE EN INFORMATIQUE ET EN AUTOMATIQUE

Numerical evaluation of a non-conforming discontinuous Galerkin method on triangular meshes for solving the time-domain Maxwell equations

Hassan Fahs

N° 6311

August 2007

Thème NUM

ISSN 0249-6399 ISRN INRIA/RR--6311--FR+ENG

INRIA
SOPHIA ANTIPOLIS

Numerical evaluation of a non-conforming discontinuous Galerkin method on triangular meshes for solving the time-domain Maxwell equations

Hassan Fahs *

Thème NUM — Systèmes numériques
Projet Nachos

Rapport de recherche n° 6311 — August 2007 — 48 pages

Abstract: We report on a detailed numerical evaluation of the non-dissipative, non-conforming discontinuous Galerkin method on triangular meshes previously introduced in [15], and further extended in [16], for solving the two-dimensional time-domain Maxwell equations. In [16], a *hp*-like DGTD (Discontinuous Galerkin Time-Domain) method is considered, where the interpolation degree is defined at the element level and the mesh is refined locally in a non-conforming way. The resulting DGTD-$\mathbb{P}_{p_c}$:$\mathbb{P}_{p_f}$ method combines a centered approximation for the evaluation of fluxes at the interface between neighboring elements of the mesh, with a second order leap-frog time integration scheme. Moreover, non-conforming meshes with arbitrary-level hanging nodes are allowed. Here, our objective is to assess the convergence, the stability and the efficiency of the method, but also discuss its limitations, through numerical experiments for 2D propagation problems in homogeneous and heterogeneous media with various types and locations of material interfaces.

Key-words: Maxwell's equations, time-domain, discontinuous Galerkin method, non-conforming triangular meshes, *hp*-like method.

* INRIA Sophia Antipolis, NACHOS project-team, Hassan.Fahs@sophia.inria.fr

Unité de recherche INRIA Sophia Antipolis
2004, route des Lucioles, BP 93, 06902 Sophia Antipolis Cedex (France)
Téléphone : +33 4 92 38 77 77 — Télécopie : +33 4 92 38 77 65

Evaluation numérique d'une méthode Galerkin discontinue non-conforme en maillages triangulaires pour la résolution des équations de Maxwell instationnaires

Résumé : Dans cette étude, on réalise une évaluation numérique détaillée de la méthode Galerkin discontinue non-conforme en maillages triangulaires pour la résolution des équations de Maxwell instationnaires précédemment introduite dans [15], puis étendue dans [16]. Dans la méthode considérée dans [16], l'ordre d'interpolation p et le pas du maillage h varient localement. La méthode DGTD-$\mathbb{P}_{p_c}$:$\mathbb{P}_{p_f}$ résultante combine une approximation centrée pour l'évaluation des flux aux interfaces entre éléments voisins du maillage, à un schéma d'intégration en temps de type saute-mouton. De plus, cette méthode autorise l'utilisation de maillages non-conformes possédant un nombre arbitraire de noeuds flottants. On présente ici les résultats d'une série d'expériences numériques pour évaluer la convergence, la stabilité et l'éfficacité de la méthode, mais aussi identifier ses limitations. Ces tests numériques sont effectués en deux dimensions d'espace et dans des milieux homogènes et hétérogènes avec différents types et différentes localisations d'interfaces entre matériaux.

Mots-clés : équations de Maxwell, domain temporel, méthode Galerkin discontinue, maillages triangulaires non-conformes, méthode *hp*.

1 Introduction

The difficulties linked to the numerical solution of the time-domain Maxwell equations find their roots in the characteristics of the underlying wave propagation problems *i.e.* the geometrical characteristics of the diffracting objects, the physical characteristics of the propagation medium (heterogeneity, physical dispersion and dissipation) and the characteristics of the sources (wires, etc.). Applications with such characteristics can be found throughout the applied sciences and engineering *e.g.* the design and optimization of antennas [7] and radars [28], the design of emerging technologies such as high speed electronics and integrated optics, and a variety of military and civilian applications [29]-[27]. Other challenging applications are addressing societal questions such as the potential adverse effects of electromagnetic waves emitted by mobile phones [31]. Such problems require high fidelity numerical solutions with a rigorous control of the numerical errors. Even for linear problems such conditions force one to look beyond standard computational techniques and seek new computational frameworks enabling the accurate, efficient, and robust modeling of wave phenomena over long simulation times in settings of realistic geometric complexity.

The simplicity and reasonable accuracy of the classical finite difference time-domain (FDTD) method [39] has propelled this method to become the method of choice among engineers and scientists solving Maxwell's equations in the time-domain. In particular the last decade has seen an increased number of applications and further developments of this method, many driven from the very influential texts by Taflove [33]. It is however clear that the original FDTD method has several limitations. Its inherent second order accuracy limits its ability to correctly represent wave motion over long distances unless the grid is prohibitively fine. Furthermore, the simplicity of the method, often recognized as its strength, also becomes its most severe restriction by prohibiting the accurate representation of problems in complex geometries. In recent years, a number of efforts aimed at addressing the shortcomings of the classical FDTD scheme, *e.g.* embedding schemes to overcome staircasing [13]-[37], high order finite difference schemes [33]-[19], non-conforming orthogonal FDTD methods [10]. Other techniques and improvements are discussed in [33]. Most of these methods, however, have not really penetrated into main stream user community, partly due to their complicated nature and partly because these new methods themselves often introduce other complications.

Finite element time-domain (FETD) methods can handle unstructured meshes and complex geometries but the development of such methods for solving Maxwell's equations, especially those with high order accuracy, has been relatively slow. A primary reason is the appearance of spurious, non-physical solutions when a straightforward nodal continuous Galerkin finite element scheme is used to approximate the Maxwell curl-curl equations. Bossavit made the fundamental observation that the use of special curl-conforming elements [24] would overcome the problem of spurious modes by mimicking properties of vector algebra [4]. Although very successful, such formulations are not entirely void of problems: the algebraic problems are larger than for nodal elements and the conformity requirements of the continuous Galerkin formulation makes adaptivity complex.

In an attempt to offer an alternative to the classical finite element formulation based on edge elements, we consider here discontinuous Galerkin formulations [8] based on high order nodal interpolation for solving the first order time-domain Maxwell's equations. Discontinuous Galerkin time-domain (DGTD) methods based on discontinuous finite element spaces, easily handle elements of various types and shapes, irregular non-conforming meshes [15], and even locally varying polynomial degree, and hence offer great flexibility in the mesh design, but they also lead to (block-) diagonal mass matrices and therefore yield fully explicit, inherently parallel methods when coupled with explicit time stepping [3]. In fact, for constant material coefficients, the mass matrix is diagonal for a judicious choice of (locally orthogonal) shape functions [30]. Moreover, continuity is weakly enforced across mesh interfaces by adding suitable bilinear forms (so-called numerical fluxes) to the standard variational formulations. Whereas high order discontinous Galerkin time-domain methods have been developed on conforming hexahedral [9] and tetrahedral [18] meshes, the design of non-conforming discontinuous Galerkin time-domain methods is still in its in-

fancy. In practice, the non-conformity can result from a local refinement of the mesh (*i.e.* h-refinement), of the interpolation degree (*i.e.* p-enrichment) or of both of them (*i.e.* hp-refinement).

This work is a continuation of [16] where a hp-like DGTD-$\mathbb{P}_{p_c}$:$\mathbb{P}_{p_f}$ method was introduced for solving the two-dimensional time-domain Maxwell equations on non-conforming triangular meshes. It was numerically shown that the proposed method has many advantages by comparing it with a h-refinement one. The main goals of this report are, on one hand, to study numerically the convergence of the h- and hp-refinement DGTD methods for propagation problems in both homogeneous and heterogeneous media and using conforming and non-conforming meshes and, on the other hand, to compare these methods in terms of accuracy and computational costs. The rest of this report is organized as follows. In section 2 we recall the basic features of our discontinuous Galerkin time-domain formulation for solving the first order Maxwell equations in the time domain, based on totally centered numerical fluxes and a leap-frog time-integration scheme. Numerical experiments are presented in section 3 for homogeneous media and section 4 for heterogeneous domain. Finally, conclusions and future works are summarized in section 5.

2 The discontinuous Galerkin scheme

We shall consider the solution of the two-dimensional Maxwell equations in the TMz polarization on a bounded domain $\Omega \subset \mathbb{R}^2$.

$$\begin{cases} \epsilon \dfrac{\partial E_z}{\partial t} - \dfrac{\partial H_y}{\partial x} + \dfrac{\partial H_x}{\partial y} = 0, \\ \mu \dfrac{\partial H_x}{\partial t} + \dfrac{\partial E_z}{\partial y} = 0, \\ \mu \dfrac{\partial H_y}{\partial t} - \dfrac{\partial E_z}{\partial x} = 0, \end{cases} \tag{2.1}$$

where the unknowns $\mathbf{E} = (0, 0, E_z)$ and $\mathbf{H} = (H_x, H_y, 0)$ are the electric and magnetic fields respectively. The electric permittivity ϵ and the magnetic permeability μ of the medium are assumed to be piecewise constant. Moreover, we assume that the field components as well as the material parameters ϵ and μ do not depend on the z coordinate. On the boundary $\Gamma = \partial\Omega$ we use either a perfect electric conductor condition *i.e.* $E_z = 0$, or a first order Silver-Müller absorbing boundary (*i.e.* an artificial boundary used to truncate the computational domain) condition *i.e.* $E_z = c\mu(n_y H_x - n_x H_y)$ or both of them, where c is the speed of propagation and $\vec{n} = (n_x, n_y)$ denotes the unit normal vector pointing outward to Γ.

We consider a partition $\mathcal{T}_h$ of Ω into a set of triangles T_i of size h_i with boundaries ∂T_i such that $h = \max_{T_i \in \mathcal{T}_h} h_i$. To each $T_i \in \mathcal{T}_h$ we assign an integer $p_i \geq 0$ and we collect the p_i in the vector $p = \{p_i : T_i \in \mathcal{T}_h\}$. Within this construction we admit meshes with possibly hanging nodes *i.e.* by allowing non-conforming (or irregular) meshes where element vertices can lie in the interior of edges of other elements (see Fig. 2.1). Each triangle T_i is assumed to be the image, under a smooth bijective (diffeomorphic) mapping τ_i, of a fixed reference triangle $\hat{\mathrm{T}} = \{\hat{x}, \hat{y} |\ \hat{x}, \hat{y} \geq 0; \hat{x}+\hat{y} \leq 1\}$. Assuming that T_i is a straight sided triangle defined through the coordinates of the three vertices $\mathbf{v}_1^i$, $\mathbf{v}_2^i$ and $\mathbf{v}_3^i$ (see Fig. 2.2), the correspondence between the two triangles $\hat{\mathrm{T}}$ and T_i is established through the use of the barycentric coordinates $(\lambda_1, \lambda_2, \lambda_3)$. We recall that any point $\mathbf{x}^i \in T_i$ can be expressed as a convex combination of the vertices of T_i and the mapping is simply given by $\tau_i : (\hat{x}, \hat{y}) \in \hat{\mathrm{T}} \rightarrow \mathbf{x}^i$, such that $\mathbf{x}^i(\hat{x}, \hat{y}) = \lambda_1 \mathbf{v}_1^i + \lambda_2 \mathbf{v}_2^i + \lambda_3 \mathbf{v}_3^i$, where $\lambda_1 + \lambda_2 + \lambda_3 = 1$ and $0 \leq (\lambda_1, \lambda_2, \lambda_3) \leq 1$ with $\lambda_1 = 1 - \hat{x} - \hat{y},\ \lambda_2 = \hat{x}$ and $\lambda_3 = \hat{y}$.

In the following, for a given partition $\mathcal{T}_h$ and vector p, we seek approximate solutions to (2.1) in the finite dimensional subspace $V_p(\mathcal{T}_h) := \{v \in L^2(\Omega) : v_{|T_i} \in \mathbb{P}^{p_i}(T_i)\ ,\ \forall T_i \in \mathcal{T}_h\}$, where $\mathbb{P}^{p_i}(T_i)$ denotes the space of nodal polynomials $\{\varphi_{ij}\}_{j=1}^{d_i}$ of total degree at most p_i on the element T_i. The space $V_p(\mathcal{T}_h)$ has the dimension d_i, the local number of degrees of freedom (DOF). Note that the polynomial degree, p_i, may vary from element to element in the mesh and that a function $v_h^p \in V_p(\mathcal{T}_h)$ is discontinuous across

element interfaces. By non-conforming interface we mean an interface a_{ik} which has at least one of its two vertices in a hanging node or/and $p_{i|_{a_{ik}}} \neq p_{k|_{a_{ik}}}$.

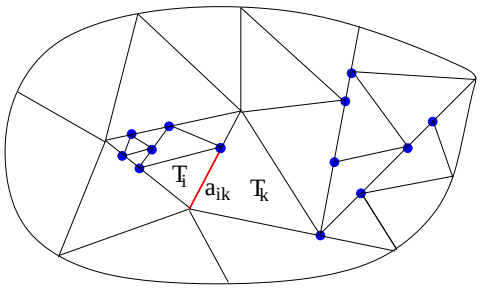

Figure 2.1: *Irregular mesh with hanging nodes.*

For each triangle T_i, ϵ_i and μ_i respectively denote the local constant electric permittivity and magnetic permeability. For two distinct triangles T_i and T_k in $\mathcal{T}_h$, the intersection $T_i \cap T_k$ is an (oriented) edge s_{ik} which we will call interface, with oriented normal vector $\vec{n}_{ik}$ and with unitary one $\vec{\widetilde{n}}_{ik}$. For the boundary interfaces, the index k corresponds to a fictitious element outside the domain. Finally, we denote by $\mathcal{V}_i$ the set of indices of the elements which are neighbors of T_i.

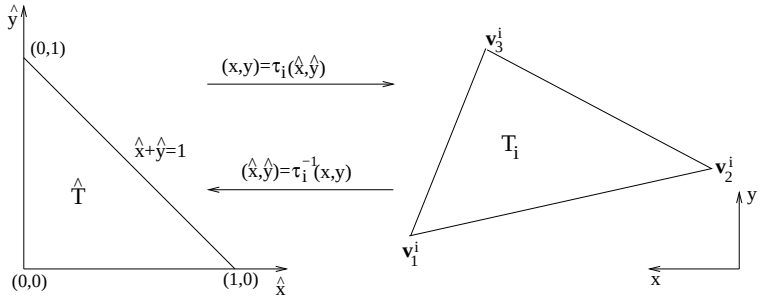

Figure 2.2: *Mapping between the physical triangle T_i and the master triangle $\hat{T}$.*

The DGTD method at the heart of this study is based on a leap-frog time scheme (E_z is computed at integer time-stations and H_x and H_y at half-integer time-stations) and totally centered numerical fluxes at the interface between elements. Decomposing H_x, H_y and E_z on element T_i according to $H_{\mathbf{x}}(.,t^{n+\frac{1}{2}}) = \sum_{j=1}^{d_i} H_{\mathbf{x}_{ij}}^{n+\frac{1}{2}} \varphi_{ij}$ and $E_z(.,t^n) = \sum_{j=1}^{d_i} E_{z_{ij}}^n \varphi_{ij}$, where $\mathbf{x} \in \{x, y\}$.

Using the notations $\mathbf{E}_{z_i}^n = (E_{z_{i1}}^n, \ldots, E_{z_{id_i}}^n)^t$ and $\mathbf{H}_{\mathbf{x}_i}^{n+\frac{1}{2}} = (H_{\mathbf{x}_{i1}}^{n+\frac{1}{2}}, \ldots, H_{\mathbf{x}_{id_i}}^{n+\frac{1}{2}})^t$, the DGTD-$\mathbb{P}_{p_i}$ method writes:

$$\left\{ \begin{array}{rcl} \epsilon_i \mathbb{M}_i \dfrac{\mathbf{E}_{z_i}^{n+1} - \mathbf{E}_{z_i}^n}{\Delta t} & = & -\mathbb{K}_i^x \mathbf{H}_{y_i}^{n+\frac{1}{2}} + \mathbb{K}_i^y \mathbf{H}_{x_i}^{n+\frac{1}{2}} + \displaystyle\sum_{k \in \mathcal{V}_i} \left(\mathbb{G}_{x_{ik}}^{n+\frac{1}{2}} - \mathbb{G}_{y_{ik}}^{n+\frac{1}{2}} \right), \\ \mu_i \mathbb{M}_i \dfrac{\mathbf{H}_{x_i}^{n+\frac{1}{2}} - \mathbf{H}_{x_i}^{n-\frac{1}{2}}}{\Delta t} & = & \mathbb{K}_i^y \mathbf{E}_{z_i}^n - \displaystyle\sum_{k \in \mathcal{V}_i} \mathbb{F}_{y_{ik}}^n, \\ \mu_i \mathbb{M}_i \dfrac{\mathbf{H}_{y_i}^{n+\frac{1}{2}} - \mathbf{H}_{y_i}^{n-\frac{1}{2}}}{\Delta t} & = & -\mathbb{K}_i^x \mathbf{E}_{z_i}^n + \displaystyle\sum_{k \in \mathcal{V}_i} \mathbb{F}_{x_{ik}}^n, \end{array} \right.$$

where $\mathbb{M}_i$ is the local mass (symmetric positive definite) matrix, and $\mathbb{K}_i^{\mathbf{x}}$ is the (skew-symmetric) stiffness matrix. The vector quantities $\mathbb{F}_{\mathbf{x}_{ik}}^n$ and $\mathbb{G}_{\mathbf{x}_{ik}}^{n+\frac{1}{2}}$ are defined as:

$$\mathbb{F}^n_{\mathbf{x}_{ik}} = \mathbb{S}^{\mathbf{x}}_{ik}\mathbf{E}^n_{z_k}, \quad \mathbb{G}^{n+\frac{1}{2}}_{\mathbf{x}_{ik}} = \mathbb{S}^{\mathbf{x}}_{ik}\mathbf{H}^{n+\frac{1}{2}}_{\mathbf{x}_k},$$

where $\mathbb{S}^{\mathbf{x}}_{ik}$ is the $d_i \times d_k$ interface matrix on s_{ik} which verifies ${}^t\mathbb{S}^{\mathbf{x}}_{ik} = -\mathbb{S}^{\mathbf{x}}_{ki}$ (if s_{ik} is an internal interface) and ${}^t\mathbb{S}^{\mathbf{x}}_{ik} = \mathbb{S}^{\mathbf{x}}_{ik}$ (if s_{ik} is a boundary interface). Note that, for non-conforming interfaces, we calculate the matrix $\mathbb{S}^{\mathbf{x}}_{ik}$ by using a Gauss quadrature formula [16].

In [15]-[16], a numerical dispersion was observed when a low order conforming DGTD-$\mathbb{P}_p$ ($p = 0, 1$ and $p_i = p$ everywhere) is applied. This dispersion error is not reduced notably by using a h-refinement strategy (*i.e.* by refining the mesh for a fixed p, yielding a locally non-conforming mesh). On the other hand, the dispersion error is minimized when a p-enrichment strategy (*i.e.* by increasing p for a fixed h) is used. However, the latter approach requires a large number of DOF thus increasing substantially the computing time and memory usage. In the recent work [16] a hp-like DGTD method has been proposed, where we combine the h-refinement and p-enrichment strategies. This method consists in using a high polynomial degree in the coarse (*i.e.* not refined) mesh and a low order one in the refined region. The resulting scheme is referred to as a DGTD-$\mathbb{P}_{p_c}$:$\mathbb{P}_{p_f}$ (or hp-refinement) method where p_c and p_f are the polynomial degrees in the coarse and fine elements respectively. We have numerically demonstrated that the DGTD-$\mathbb{P}_{p_c}$:$\mathbb{P}_{p_f}$ method can strongly reduce, in the one hand, the dispersion error and, in the other hand, the computational cost and memory consumption compared with the h-refinement method. Of course, such a non-conforming scheme is a first step towards a fully hp-adaptive method relying on appropriate error estimators.

The stability of the DGTD-$\mathbb{P}_{p_i}$ method for non-conforming meshes is studied in [15] using an energetic approach. Furthermore, a theoretical proof of the convergence has been established in [18] for any interpolation degree $p \neq 0$ in the case of conforming simplicial meshes. It is shown that the convergence rate of DGTD-$\mathbb{P}_p$ method is $\mathcal{O}(Th^{\min(s,p)}) + \mathcal{O}(\Delta t^2)$, where Δt is the time step over the interval $[0, T]$ and the solution belongs to $H^s(\Omega)$ with $s > 1/2$. Our attention is turned on the validity of this result in the case of non-conforming meshes using the DGTD-$\mathbb{P}_p$ and DGTD-$\mathbb{P}_{p_c}$:$\mathbb{P}_{p_f}$ methods, and an answer is given here on the basis of numerical simulations.

3 Homogeneous media

In this section, we consider several wave propagation problems in homogeneous media for which analytical solutions exist. Our objectives are the following:

- to assess numerically and compare the convergence of the conforming and non-conforming DGTD methods,
- to provide insights regarding the overall performances of the hp-refinement DGTD-$\mathbb{P}_{p_c}$:$\mathbb{P}_{p_f}$ method,
- to compare, on one hand, the conforming DGTD-$\mathbb{P}_p$ method with the non-conforming one and, on the other hand, the hp-refinement method with the h-refinement one.

The above points are studied for the following test cases:

1. a concentric PEC cylinders resonator,
2. a circular PEC resonator,
3. a wedge-shaped PEC resonator.

3.1 Concentric PEC cylinders resonator

We consider a resonator which consists of two concentric PEC cylinders with an electromagnetic wave bouncing back and forth between the walls (see Fig. 3.1). The material is taken to be the vacuum *i.e.* $\epsilon = \mu = 1$ (relative quantities). The radii of the two cylinders are $r_1 = \frac{1}{6}$ and $r_2 = \frac{1}{2}$. The exact time-domain solution of the problem is [12]-[13]:

$$
\begin{aligned}
E_z &= \cos(\omega t + \theta)[J_1(\omega r) + aY_1(\omega r)], \\
H_x &= -\frac{1}{2}\sin(\omega t + \theta)\sin(\theta)[J_0(\omega r) - J_2(\omega r) + a(Y_0(\omega r) - Y_2(\omega r))] \\
&\quad -\frac{\cos(\theta)}{\omega r}\cos(\omega t + \theta)[J_1(\omega r) + aY_1(\omega r)], \\
H_y &= \frac{1}{2}\sin(\omega t + \theta)\cos(\theta)[J_0(\omega r) - J_2(\omega r) + a(Y_0(\omega r) - Y_2(\omega r))] \\
&\quad -\frac{\sin(\theta)}{\omega r}\cos(\omega t + \theta)[J_1(\omega r) + aY_1(\omega r)],
\end{aligned}
$$

for $r_1 < r < r_2$, where $(r,\ \theta) = (\sqrt{x^2 + y^2},\ \arctan(y/x))$ are the usual polar coordinates; J_n and Y_n stand for the n-th order Bessel functions of the first and second kind, respectively. The values of the parameters ω and a are obtained by enforcing the boundary condition $E_z = 0$ at $r = r_1$ and $r = r_2$. Then, as in [12], we set $\omega = 9.813695999428405$ and $a = 1.76368380110927$. First, a quasi-uniform conforming mesh is constructed (see Fig. 3.2 left). Then a non-conforming mesh is obtained by locally refining a cylindrical zone as shown on Fig. 3.2 right. Contour lines of the E_z component at times $t = 1$ and $t = 10$ are shown on Fig. 3.3 for a calculation based on the conforming DGTD-$\mathbb{P}_1$ method.

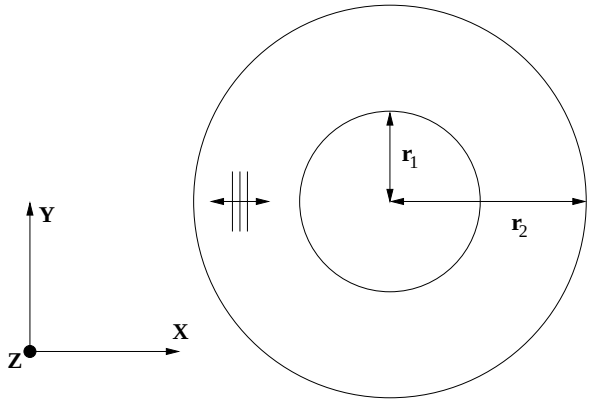

Figure 3.1: *Concentric PEC cylinders resonator setting.*

Two strategies are considered for this problem: the first one is the DGTD-$\mathbb{P}_p$ (or h-refinement) method and the second one is the DGTD-$\mathbb{P}_{p_c}$:$\mathbb{P}_{p_f}$ (or hp-refinement) method.

h-refinement DGTD-$\mathbb{P}_p$ method. We first consider the case where the interpolation degree p is uniform and the mesh size h is varied. In Tab. 3.1, we summarize the CFL values evaluated numerically for some p (*i.e.* by assessing the limit beyond which we observe a growth of the discrete energy). Tab. 3.2 and 3.3 give the L^2 error on the electric field component E_z, the convergence rate, the CPU time and the number of time steps (# time steps) to reach $t = 1$ and using sequences of conforming and non-conforming

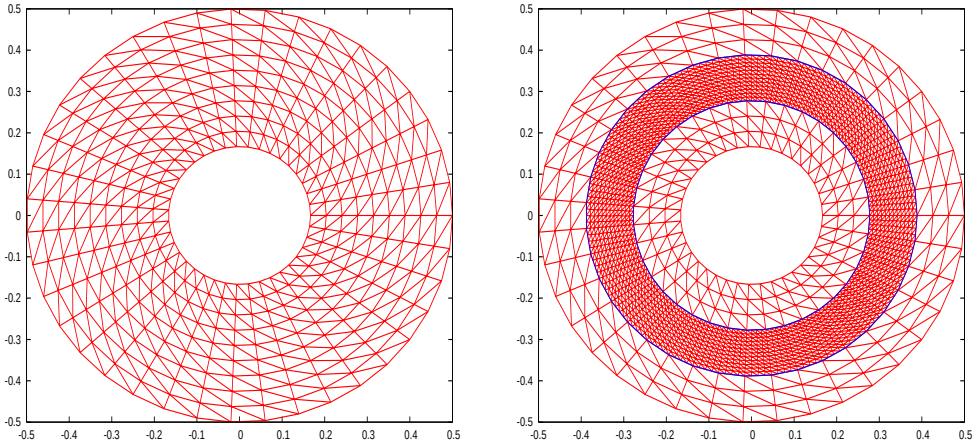

Figure 3.2: *Concentric cylinders PEC resonator.*
Example of conforming (left) and non-conforming (right) triangular meshes.

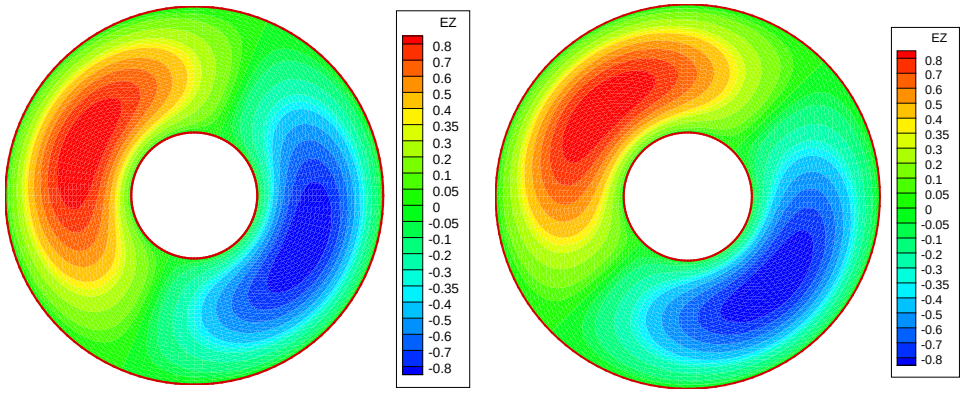

Figure 3.3: *Concentric cylinders PEC resonator.*
Contour lines of E_z *at* $t = 1$ *(left) and* $t = 10$ *(right).*
DGTD-$\mathbb{P}_1$ *method using a conforming mesh with* 1088 *nodes and* 2048 *triangles.*

meshes. The characteristics of these meshes are also listed in Tab. 3.2 and 3.3. The non-conforming meshes are obtained by refining (one refinement level) the cylindrical zone $1/3 \leq r \leq 3/8$. Fig. 3.4 shows the L^2 error on E_z as a function of the square root of the number of degrees of freedom (# DOF). We can deduce from Tab. 3.2 and 3.3 that the DGTD-$\mathbb{P}_p$ method converges as $h^{(2)}$ $\forall p \geq 1$ and as $h^{(1)}$ for $p = 0$, for conforming as well as non-conforming meshes.

Table 3.1: *Concentric cylinders PEC resonator. Numerical CFL values for the DGTD-$\mathbb{P}_p$ method.*

p	0	1	2	3	4
CFL	1.0	0.3	0.2	0.1	0.09

Table 3.2: *Concentric cylinders PEC resonator. Convergence study for the h-refinement DGTD-$\mathbb{P}_p$ method using conforming meshes. L^2 error, CPU time and # time steps are measured at $t = 1$.*

Characteristics of the conforming meshes. # nodes	# triangles	# DOF	L^2 error	convergence rate	CPU (s)	# time steps
		DGTD-$\mathbb{P}_0$				
1088	2048	2048	5.24E−02	–	2	80
4224	8192	8192	2.62E−02	1.00	9	158
16640	32768	32768	1.31E−02	1.00	74	313
66048	131072	131072	6.56E−03	1.00	593	624
		DGTD-$\mathbb{P}_1$				
288	512 (mesh-A [a])	1536	2.52E−02	–	2	137
1088	2048 (mesh-B)	6144	6.46E−03	1.96	9	266
4224	8192 (mesh-C)	24576	1.65E−03	1.97	65	525
16640	32768 (mesh-D)	98304	4.11E−04	2.00	524	1043
		DGTD-$\mathbb{P}_2$				
	mesh-A	3072	1.44E−02	–	3	205
	mesh-B	12288	3.58E−03	2.01	21	399
	mesh-C	49152	8.93E−04	2.00	168	787
	mesh-D	196608	2.23E−04	2.00	1390	1564
		DGTD-$\mathbb{P}_3$				
	mesh-A	5120	1.42E−02	–	10	410
	mesh-B	20480	3.52E−03	2.02	71	797
	mesh-C	81920	8.74E−04	2.01	565	1574
	mesh-D	327680	2.18E−04	2.01	4916	3128

[a] This means that mesh-A contains 288 nodes and 512 triangles, etc.

***hp*-refinement DGTD-$\mathbb{P}_{p_c}$:$\mathbb{P}_{p_f}$ method.** We now consider the case where both p and h are locally refined. The observed numerical CFL values for the DGTD-$\mathbb{P}_{p_c}$:$\mathbb{P}_{p_f}$ method are summarized in Tab. 3.4. We give in Tab. 3.5, the L^2 error on E_z, the convergence rate, the CPU time and the number of time steps to reach $t = 1$ using non-conforming meshes which are obtained by refining the zone $1/3 \leq r \leq 3/8$ as previously. Fig. 3.5 shows the L^2 error on E_z as a function of the square root of the number of DOF. Clearly, the DGTD-$\mathbb{P}_{p_c}$:$\mathbb{P}_{p_f}$ method converges as $h^{(2)}$, $\forall p_f \neq 0$, and for $p_f = 0$ the convergence rate is more than $\mathcal{O}(h^{(1.5)})$, $\forall p_c$.

In summary, the results given in Tab. 3.2, 3.3 and 3.5 motivates the following remarks:

- in the case of the h-refinement DGTD-$\mathbb{P}_p$ method using both conforming and non-conforming meshes, it is not necessary to increase the interpolation degree p to more than 2. Clearly, doing so

Table 3.3: *Concentric cylinders PEC resonator.*
Convergence study for the h-refinement DGTD-$\mathbb{P}_p$ method using non-conforming meshes.
L^2 error, CPU time and # time steps are measured at $t = 1$.

Characteristics of the non-conforming meshes. # nodes	# hanging nodes	# triangles	# DOF	L^2 error	convergence rate	CPU (s)	# time steps
		DGTD-$\mathbb{P}_0$					
1536	128	2816	2816	5.49E−02	–	3	117
5888	256	11264	11264	2.75E−02	1.00	19	231
23040	512	45056	45056	1.37E−02	1.00	155	458
91136	1024	180224	180224	6.86E−03	1.00	1270	913
		DGTD-$\mathbb{P}_1$					
416	64	704 (mesh-E [a])	2112	2.27E−02	–	3	199
1536	128	2816 (mesh-F)	8448	5.83E−03	1.97	17	389
5888	256	11264 (mesh-G)	33792	1.48E−03	1.98	131	768
23040	512	45056 (mesh-H)	135168	3.73E−04	1.99	1071	1526
		DGTD-$\mathbb{P}_2$					
		mesh-E	4224	1.42E−02	–	6	299
		mesh-F	16896	3.52E−03	2.01	43	583
		mesh-G	67584	8.75E−04	2.01	347	1151
		mesh-H	270336	2.18E−04	2.00	2842	2289
		DGTD-$\mathbb{P}_3$					
		mesh-E	7040	1.41E−02	–	18	597
		mesh-F	28160	3.50E−03	2.01	144	1165
		mesh-G	112640	8.69E−04	2.01	1148	2302
		mesh-H	450560	2.17E−04	2.01	9466	4578

[a] This means that mesh-E contains 416 nodes in which 64 are hanging nodes, and 704 triangles, etc.

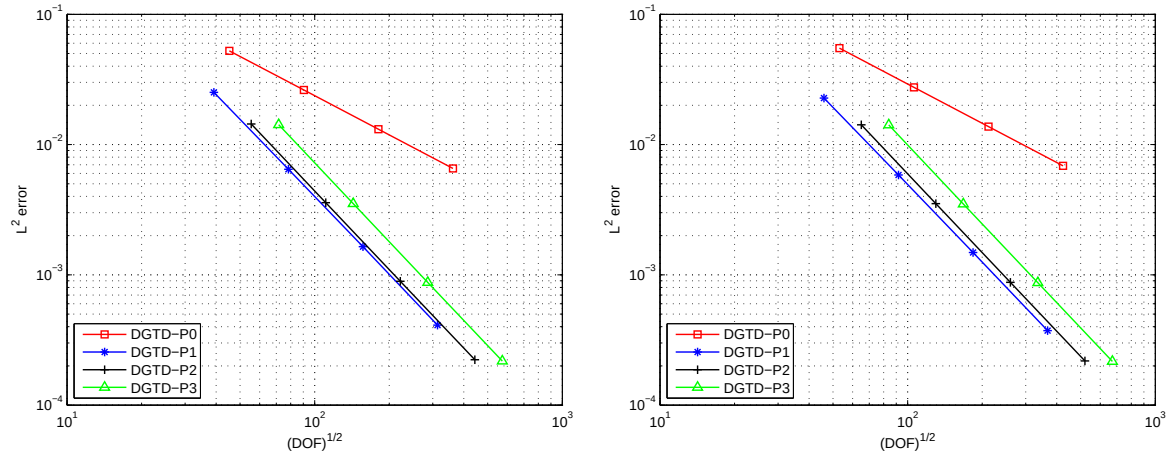

Figure 3.4: *Concentric cylinders PEC resonator.*
Numerical convergence of the h-refinement DGTD-$\mathbb{P}_p$ method.
Conforming (left) and non-conforming (right) triangular meshes.

Table 3.4: *Concentric cylinders PEC resonator.*
Numerical CFL values for the DGTD-$\mathbb{P}_{p_c}$:$\mathbb{P}_{p_f}$ method.

$p_c : p_f$	1 : 0	2 : 0	2 : 1	3 : 0	3 : 1	3 : 2	4 : 2	4 : 3
CFL	0.5	0.3	0.3	0.19	0.19	0.19	0.1	0.1

Table 3.5: *Concentric cylinders PEC resonator. Convergence study of the DGTD-$\mathbb{P}_{p_c}$:$\mathbb{P}_{p_f}$ method. Non-conforming locally refined meshes. L^2 error, CPU time and # time steps are measured at $t = 1$.*

mesh[a]	% DOF$_f$[b]	# DOF	L^2 error	convergence rate	CPU (s)	# time steps
			DGTD-$\mathbb{P}_1$:$\mathbb{P}_0$			
mesh-E	16%	1600	2.51E−02	–	2	120
mesh-F	16%	6400	7.89E−03	1.67	8	233
mesh-G	16%	25600	2.11E−03	1.90	64	461
mesh-H	16%	102400	7.08E−04	1.58	527	916
			DGTD-$\mathbb{P}_2$:$\mathbb{P}_0$			
mesh-E	9%	2944	1.90E−02	–	3	199
mesh-F	9%	11776	7.11E−03	1.42	21	389
mesh-G	9%	47104	1.91E−03	1.89	168	768
mesh-H	9%	188416	7.58E−04	1.33	1394	1526
			DGTD-$\mathbb{P}_3$:$\mathbb{P}_0$			
mesh-E	5%	4736	1.90E−02	–	7	315
mesh-F	5%	18944	6.29E−03	1.60	53	613
mesh-G	5%	75776	2.14E−03	1.56	421	1212
mesh-H	5%	303104	8.52E−04	1.33	3445	2410
			DGTD-$\mathbb{P}_2$:$\mathbb{P}_1$			
mesh-E	22%	3456	1.49E−02	–	4	199
mesh-F	22%	13824	3.71E−03	2.00	25	389
mesh-G	22%	55296	9.23E−04	2.01	194	768
mesh-H	22%	221184	2.30E−04	2.00	1597	1526
			DGTD-$\mathbb{P}_3$:$\mathbb{P}_1$			
mesh-E	15%	5248	1.48E−02	–	8	299
mesh-F	15%	20992	3.66E−03	2.01	55	583
mesh-G	15%	83968	9.11E−04	2.01	461	1212
mesh-H	15%	335872	2.27E−04	2.00	3775	2410
			DGTD-$\mathbb{P}_3$:$\mathbb{P}_2$			
mesh-E	26%	6016	1.42E−02	–	8	299
mesh-F	26%	24064	3.53E−03	2.02	63	583
mesh-G	26%	96256	8.76E−04	2.01	526	1212
mesh-H	26%	385024	2.18E−04	2.01	4262	2410
			DGTD-$\mathbb{P}_4$:$\mathbb{P}_2$			
mesh-E	19%	8256	1.42E−02	–	21	597
mesh-F	19%	33024	3.50E−03	2.02	165	1165
mesh-G	19%	132096	8.70E−04	2.01	1340	2302
mesh-H	19%	528384	2.17E−04	2.01	10955	4578
			DGTD-$\mathbb{P}_4$:$\mathbb{P}_3$			
mesh-E	28%	9280	1.42E−02	–	24	597
mesh-F	28%	37120	3.50E−03	2.02	188	1165
mesh-G	28%	148480	8.70E−04	2.01	1501	2302
mesh-H	28%	593920	2.16E−04	2.00	12254	4578

[a] See Tab. 3.3 for the characteristics of these meshes.
[b] Represents the percentage of the DOF in the fine mesh.

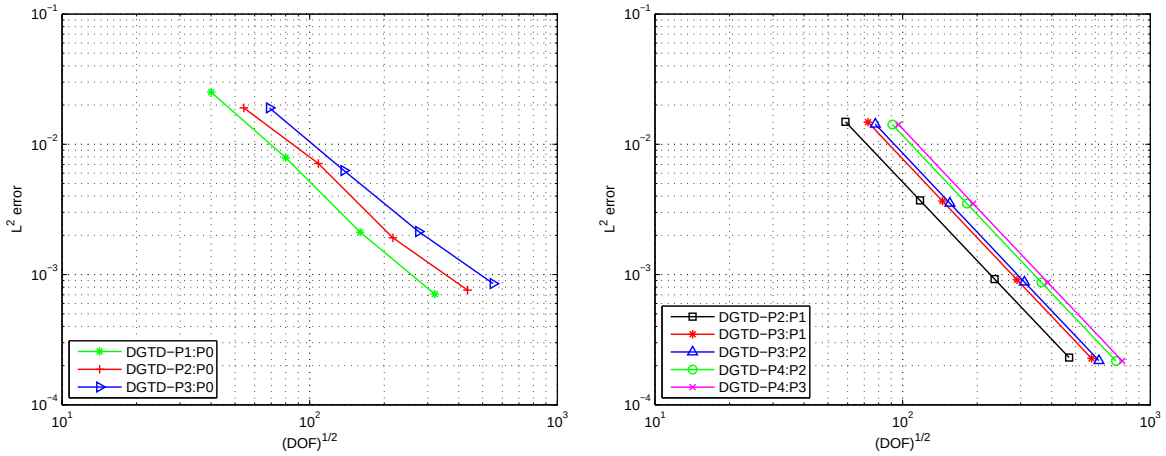

Figure 3.5: *Concentric cylinders PEC resonator. Numerical convergence of the hp-refinement DGTD-$\mathbb{P}_{p_c}$:$\mathbb{P}_{p_f}$ method. Non-conforming triangular meshes.*

does not improve the convergence rate. Furthermore, to reach a given error level, the DGTD-$\mathbb{P}_3$ is more expensive than the DGTD-$\mathbb{P}_2$ method.

- for a given p, the conforming DGTD-$\mathbb{P}_p$ method always requires less computing time than the non-conforming one. In fact, a comparison of the two methods from the point of view of the CPU time is rather unfair in the present case since the local refinement of the mesh is performed arbitrarily (*i.e.* not motivated by any physical or geometrical concern).

- in general, for a given error level $< 10^{-2}$ the *hp*-refinement method is less expensive than the *h*-refinement one. For example, if we use the DGTD-$\mathbb{P}_{p_c}$:$\mathbb{P}_0$ method for $p_c = 1, 2, 3$ respectively, rather than the DGTD-$\mathbb{P}_0$ method, the gains in the number of DOF and CPU time vary from 95% to 85%. Similarly, the DGTD-$\mathbb{P}_2$:$\mathbb{P}_1$ method can be compared with the DGTD-$\mathbb{P}_p$ one for $p = 1, 2$.

- finally, we have observed that, in the case of the DGTD-$\mathbb{P}_{p_c}$:$\mathbb{P}_{p_f}$ method, it is not reasonable to increase the interpolation degree p_c in the coarse mesh to more than $p_f + 1$ since doing so does not improve the convergence rate and results in increased CPU time and memory usage.

Comparison with various FDTD methods. Here we compare the DGTD-$\mathbb{P}_0$ method with two different FDTD schemes:

1. the classical second order Yee scheme [39] staggered both in space and time where the numerical solution is carried out on a *staircased* mesh;

2. a modification of the Yee scheme (refered as Ty(2,4)), see [35]-[36], and chapter 2 in [33]. This method is fourth order accurate in space and second order accurate in time. The numerical solution is also computed on a stagger *staircased* mesh.

The L^2 error on the E_z component and the convergence rate of these two FDTD schemes measured at times $t = 1$ and $t = 10$ are given in Tab. 3.6. These results were taken from [1]-[38]. It is seen from Tab. 3.6 that the staircased FDTD approximation leads to an extremely slow convergence rate at early time ($t = 1$) and a divergent scheme at late time ($t = 10$). According to [38], this is probably not only because the staircasing misrepresents the shape of the cylinders, but also because of the fact that in this resonator case an electromagnetic wave is bouncing back and forth between the walls, so numerical errors accumulate quickly in the solution. These FDTD results are compared with the classical centered

finite volume DGTD-$\mathbb{P}_0$ scheme on conforming triangular meshes (see Tab. 3.6). One can see that the DGTD-$\mathbb{P}_0$ conserves a linear convergence rate even for a long simulation time.

Table 3.6: *Concentric cylinders PEC resonator. The L^2 error on E_z for two different FDTD schemes and for the DGTD-$\mathbb{P}_0$ method.*

t=1			t=10		
Yee scheme (staircased) cartesian grid [a].					
grid	L^2 error	convergence rate	grid	L^2 error	convergence rate
1000	4.322E−01	–	1000	5.101E−01	–
4000	3.635E−01	0.28	4000	4.364E−01	0.23
16000	1.742E−01	1.06	16000	6.683E−01	−0.61
Ty(2,4) (staircased) cartesian grid [b].					
1000	4.038E−01	–	1000	2.642E−01	–
4000	3.347E−01	0.27	4000	7.079E−01	−1.42
16000	1.579E−01	1.08	16000	7.243E−01	−0.03
The classical centered finite volume DGTD-$\mathbb{P}_0$ scheme.					
$\sqrt{\text{DOF}}$	L^2 error	convergence rate	$\sqrt{\text{DOF}}$	L^2 error	convergence rate
90	2.62E−02	–	90	4.52E−02	–
180	1.31E−02	0.99	180	1.89E−02	1.25
360	6.65E−03	1.00	360	8.96E−03	1.08

[a] Results were taken from [1]-[38].
[b] Results were taken from [1].

3.2 Circular PEC resonator

We consider a circular PEC resonator with radius $r = 1/2$. The material is taken to be the vacuum. The exact time-domain solution of the problem is [36]:

$$
\begin{aligned}
E_z &= J_1(\omega r)\cos(\omega t + \theta), \\
H_x &= \frac{y}{2r}[J_0(\omega r) - J_2(\omega r)]\cos(\omega t + \theta) - \frac{x}{\omega r^2} J_1(\omega r)\sin(\omega t + \theta), \\
H_y &= -\frac{x}{2r}[J_0(\omega r) - J_2(\omega r)]\cos(\omega t + \theta) - \frac{y}{\omega r^2} J_1(\omega r)\sin(\omega t + \theta),
\end{aligned}
$$

where $\omega = 14.03117333963124$, which is obtained from the PEC boundary condition $E_z = 0$ at $r = 1/2$. As in the previous test case, (r, θ) represent the usual polar coordinates.

Numerical simulations make use of quasi-uniform triangular meshes with possibly obtuse angles (see Fig. 3.6 left). The percentage of triangles with obtuse angles is between 45 % and 50 % which correspond to a maximum angle between 100° and 90° respectively. The non-conforming meshes are obtained by locally refining a cylindrical zone as shown on Fig. 3.6 right. Contour lines of the E_z component at times $t = 1$ and $t = 10$ are shown on Fig. 3.7 for a calculation based on the conforming DGTD-$\mathbb{P}_1$ method.

As for the previous test case, we apply the h-refinement DGTD-$\mathbb{P}_p$ and the hp-refinement DGTD-$\mathbb{P}_{p_c}$:$\mathbb{P}_{p_f}$ methods.

h-refinement DGTD-$\mathbb{P}_p$ method. For each polynomial degree p, we use four different conforming and non-conforming meshes whose characteristics are listed in Tab. 3.7 and 3.8. The non-conforming meshes are obtained by locally refining (one refinement level) the cylindrical zone $0.3 \leq r \leq 0.4$ of the conforming meshes. We use here the same CFL values as in the previous example (see Tab. 3.1). We

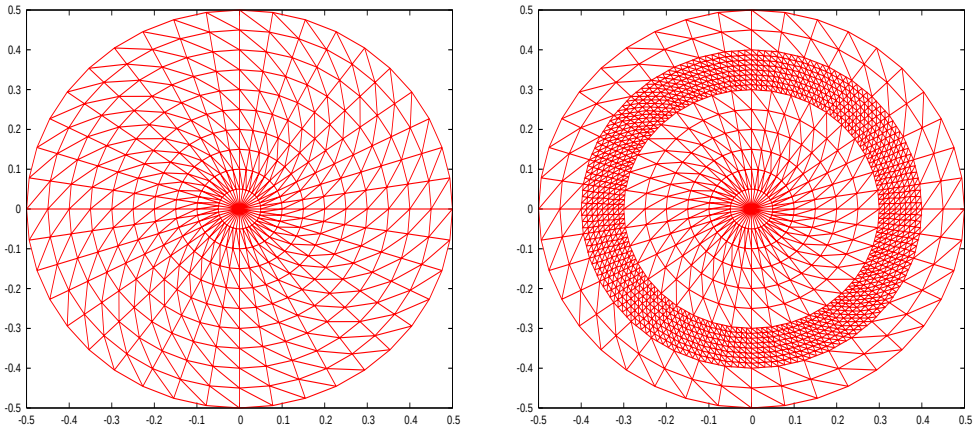

Figure 3.6: *Circular PEC resonator.*
Example of conforming (left) and non-conforming (right) triangular meshes.

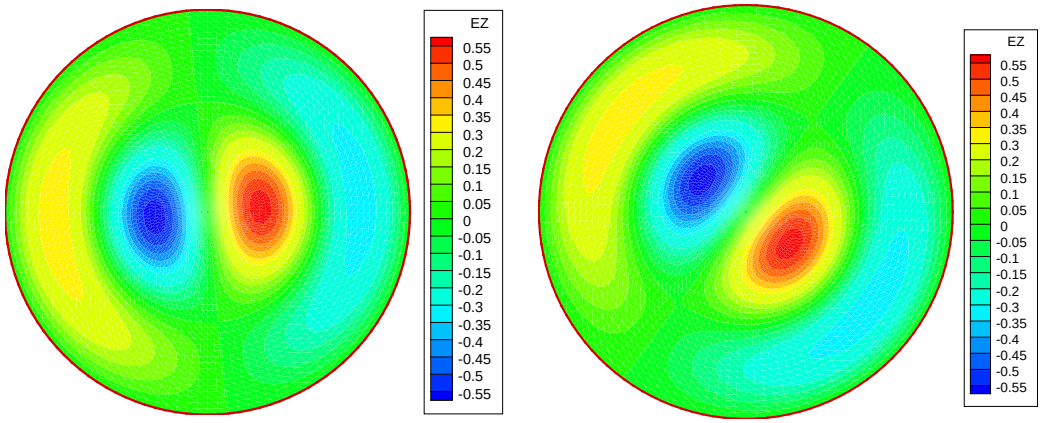

Figure 3.7: *Circular PEC resonator.*
Contour lines of E_z *at* $t = 1$ *(left) and* $t = 10$ *(right).*
DGTD-$\mathbb{P}_1$ *method using a conforming mesh with* 4201 *nodes and* 8280 *triangles.*

give in Tab. 3.7 and 3.8 the L^2 error on E_z, the convergence rate, the CPU time and the number of time steps to reach $t = 0.8$. Fig. 3.8 shows the corresponding L^2 error as a function of the square root of the number of DOF. We can deduce from Tab. 3.7 and 3.8 that for conforming as well as non-conforming meshes, the DGTD-$\mathbb{P}_p$ method converges as $h^{(2)}$ for $p \geq 1$ and as $h^{(1)}$ for $p = 0$.

Table 3.7: *Circular PEC resonator.*
Convergence study for the h-refinement DGTD-$\mathbb{P}_p$ method using conforming meshes.
L^2 error, CPU time and # time steps are measured at $t = 0.8$.

Characteristics of the conforming meshes. # nodes	# triangles	# DOF	L^2 error	convergence rate	CPU (s)	# time steps
		DGTD-$\mathbb{P}_0$				
176	325 (mesh-A)	325	6.73E−02	–	< 1	48
701	1350 (mesh-B)	1350	2.88E−02	1.19	2	182
2801	5500 (mesh-C)	5500	1.34E−02	1.08	24	717
11201	22200 (mesh-C)	22200	6.58E−03	1.02	417	2856
		DGTD-$\mathbb{P}_1$				
	mesh-A	975	4.45E−02	–	< 1	160
	mesh-B	4050	1.21E−02	1.83	10	606
	mesh-C	16500	3.07E−03	1.95	169	2388
	mesh-D	66600	7.76E−04	1.97	2855	9518
		DGTD-$\mathbb{P}_2$				
	mesh-A	1950	1.32E−02	–	2	239
	mesh-B	8100	3.19E−03	2.00	26	908
	mesh-C	33000	7.89E−04	1.99	432	3582
	mesh-D	133200	1.96E−04	1.99	7229	14277
		DGTD-$\mathbb{P}_3$				
	mesh-A	3250	1.29E−02	–	7	478
	mesh-B	13500	3.17E−03	1.97	86	1816
	mesh-C	55000	7.88E−04	1.98	1450	7163
	mesh-D	222000	1.97E−04	1.99	24190	28554

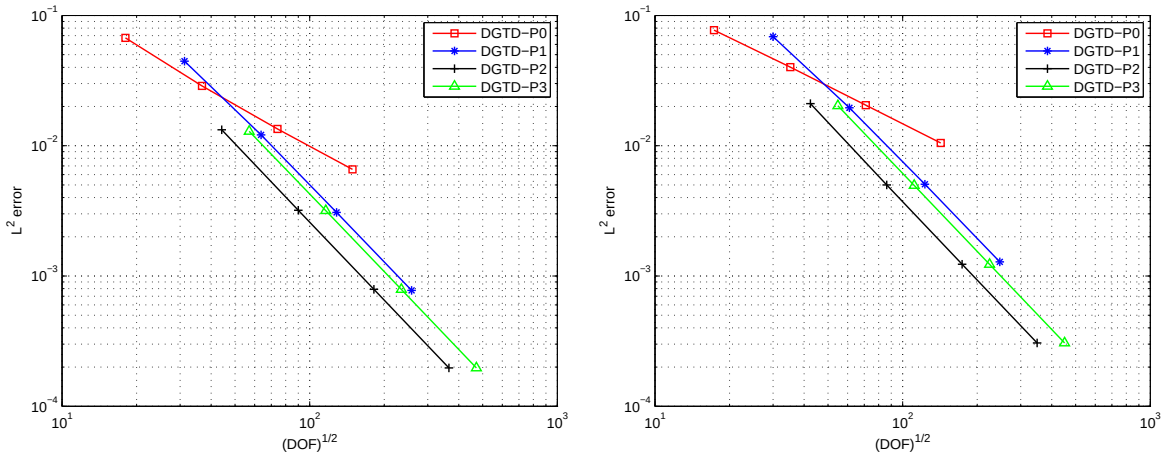

Figure 3.8: *Circular PEC resonator.*
Numerical convergence of the h-refinement DGTD-$\mathbb{P}_p$ method.
Conforming (left) and non-conforming (right) triangular meshes.

Table 3.8: *Circular PEC resonator.*
Convergence study for the h-refinement DGTD-$\mathbb{P}_p$ method using non-conforming meshes.
L^2 error, CPU time and # time steps are measured at $t = 0.8$.

Characteristics of the non-conforming meshes. # nodes	# hanging nodes	# triangles	# DOF	L^2 error	convergence rate	CPU (s)	# time steps
		DGTD-$\mathbb{P}_0$					
181	40	300 (mesh-E)	300	7.71E−02	–	$<< 1$	29
681	80	1240 (mesh-F)	1240	4.01E−02	0.92	1	105
2641	160	5040 (mesh-G)	5040	2.05E−02	0.96	12	411
10401	320	20320 (mesh-H)	20320	1.05E−02	0.96	224	1633
		DGTD-$\mathbb{P}_1$					
		mesh-E	900	6.87E−02	–	< 1	95
		mesh-F	3720	1.96E−02	1.77	6	350
		mesh-G	15120	5.07E−03	1.93	90	1368
		mesh-H	60960	1.28E−03	1.97	1484	5443
		DGTD-$\mathbb{P}_2$					
		mesh-E	1800	2.10E−02	–	2	142
		mesh-F	7440	4.99E−03	2.03	14	524
		mesh-G	30240	1.23E−03	2.00	234	2052
		mesh-H	121920	3.06E−04	2.00	3838	8164
		DGTD-$\mathbb{P}_3$					
		mesh-E	3000	2.03E−02	–	4	284
		mesh-F	12400	4.96E−03	1.98	49	1048
		mesh-G	50400	1.23E−03	1.99	782	4104
		mesh-H	203200	3.06E−04	1.99	12681	16327

***hp*-refinement DGTD-$\mathbb{P}_{p_c}$:$\mathbb{P}_{p_f}$ method.** The observed numerical CFL values of the DGTD-$\mathbb{P}_{p_c}$:$\mathbb{P}_{p_f}$ method are reported in Tab. 3.9. As with the h-refinement method, the non-conforming meshes are obtained by locally refining the cylindrical zone $0.3 \leq r \leq 0.4$. We give in Tab. 3.12 the L^2 error on E_z, the convergence rate, the CPU time and the number of time steps to reach $t = 0.8$. Fig. 3.9 shows the corresponding L^2 error on E_z as a function of the square root of the number of DOF. It is clear from Tab. 3.12 that the DGTD-$\mathbb{P}_{p_c}$:$\mathbb{P}_{p_f}$ converges as $h^{(2)}$, $\forall p_f \neq 0$ while the convergence rate for $p_f = 0$ is more than $\mathcal{O}(h^{(1.8)})$, $\forall p_c$.

Table 3.9: *Circular PEC resonator.*
Numerical CFL values for DGTD-$\mathbb{P}_{p_c}$:$\mathbb{P}_{p_f}$ method.

$p_c : p_f$	1 : 0	2 : 0	2 : 1	3 : 0	3 : 1	3 : 2	4 : 2	4 : 3
CFL	0.3	0.2	0.2	0.1	0.1	0.1	0.08	0.08

In summary, the results given in Tab. 3.7, 3.8 and 3.12 call for the following comments:

- it is not reasonable to increase the polynomial degree in the coarse mesh to more than $p_c = p_f + 1$ (see Tab. 3.10). One can clearly deduce from Tab. 3.10 that the DGTD-$\mathbb{P}_2$:$\mathbb{P}_1$ method is the least expensive *hp*-refinement method for this problem.
- the DGTD-$\mathbb{P}_2$:$\mathbb{P}_1$ method is less expensive than the non-conforming DGTD-$\mathbb{P}_p$ one. For example, we have observed (results not reported in a table here) that to obtain an error level of 0.4%, on one hand, the DGTD-$\mathbb{P}_1$ and DGTD-$\mathbb{P}_2$ method require 19500 and 8454 DOF respectively while the corresponding CPU times are 160 and 29 seconds and, on the other hand, the DGTD-$\mathbb{P}_2$:$\mathbb{P}_1$ method needs 8100 DOF and 28 seconds (see Tab. 3.10).

- the DGTD-$\mathbb{P}_2$:$\mathbb{P}_1$ method can be compared with the conforming DGTD-$\mathbb{P}_p$ one. Indeed, the results of Tab. 3.10 together with those of Tab. 3.11 show that the DGTD-$\mathbb{P}_2$:$\mathbb{P}_1$ method is less expensive than the DGTD-$\mathbb{P}_1$ and DGTD-$\mathbb{P}_3$ ones, but it is not much more expensive than the DGTD-$\mathbb{P}_2$ method. One can note here that the results of the DGTD-$\mathbb{P}_2$:$\mathbb{P}_1$ method remain very satisfactory despite that the space $\mathbb{P}_1$ is used in 53% of the triangles of the mesh.

Table 3.10: *Circular PEC resonator.*
 # DOF and CPU time to reach an error level of 0.4%.
DGTD-$\mathbb{P}_{p_c}$:$\mathbb{P}_{p_f}$ method with locally refined meshes.

DGTD-$\mathbb{P}_{p_c}$:$\mathbb{P}_{p_f}$	$\mathbb{P}_1$:$\mathbb{P}_0$	$\mathbb{P}_2$:$\mathbb{P}_0$	$\mathbb{P}_2$:$\mathbb{P}_1$	$\mathbb{P}_3$:$\mathbb{P}_0$	$\mathbb{P}_3$:$\mathbb{P}_1$	$\mathbb{P}_3$:$\mathbb{P}_2$	$\mathbb{P}_4$:$\mathbb{P}_2$	$\mathbb{P}_4$:$\mathbb{P}_3$
# DOF	25602	47088	8100	47090	12120	12150	17670	22500
# CPU (s)	320	1000	28	1200	170	157	190	201

Table 3.11: *Circular PEC resonator.*
 # DOF and CPU time to reach an error level of 0.4%.
DGTD-$\mathbb{P}_p$ method using conforming meshes.

DGTD-$\mathbb{P}_p$	DGTD-$\mathbb{P}_1$	DGTD-$\mathbb{P}_2$	DGTD-$\mathbb{P}_3$
# DOF	13689	6402	10400
# CPU (s)	100	18	59

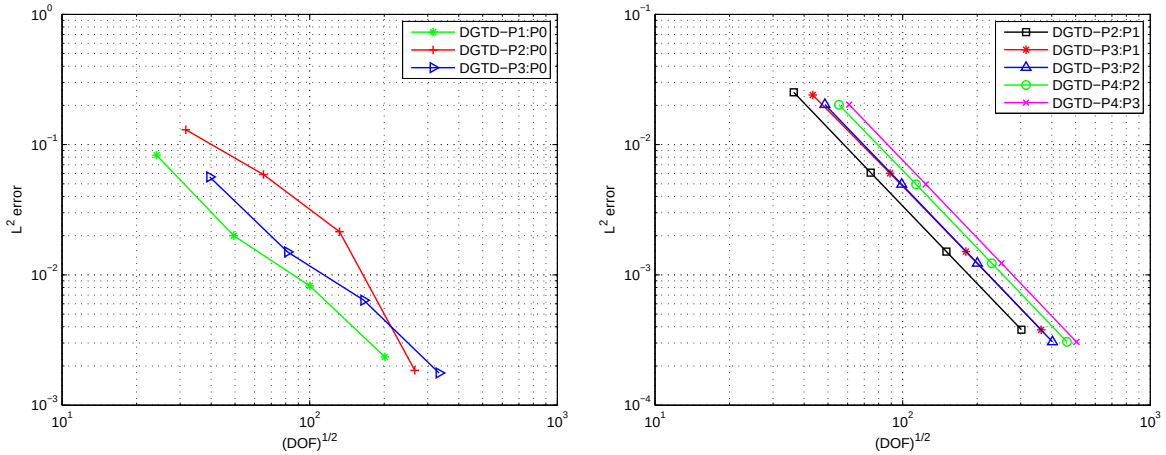

Figure 3.9: *Circular PEC resonator.*
Numerical convergence of the hp-refinement DGTD-$\mathbb{P}_{p_c}$:$\mathbb{P}_{p_f}$ method.
Non-conforming triangular meshes.

3.3 Wedge-shaped PEC resonator

We consider a computational domain which is bounded by the curves $y = \tan(\frac{3\pi}{7})x$, $x^2 + y^2 = \frac{1}{4}$ and the x-axis (see Fig. 3.10). The boundaries of the sector are assumed to be perfectly conducting. The exact time-domain solution is [36]:

Table 3.12: *Circular PEC resonator.*
Convergence study of the DGTD-$\mathbb{P}_{p_c}$:$\mathbb{P}_{p_f}$ method.
Non-conforming locally refined meshes.
L^2 error, CPU time and # time steps are measured at $t = 0.8$.

mesh[a]	% DOF$_f$[b]	# DOF	L^2 error	convergence rate	CPU (s)	# time steps
			DGTD-$\mathbb{P}_1$:$\mathbb{P}_0$			
mesh-E	28 %	580	8.30E−02	–	< 1	95
mesh-F	26 %	2440	1.99E−02	1.98	4	350
mesh-G	26 %	10000	8.25E−03	1.23	66	1368
mesh-H	25 %	40480	2.34E−03	1.80	1123	5443
			DGTD-$\mathbb{P}_2$:$\mathbb{P}_0$			
mesh-E	16 %	1000	1.30E−01	–	1	142
mesh-F	15 %	4240	5.89E−02	1.10	9	524
mesh-G	15 %	17440	2.14E−02	1.43	146	2052
mesh-H	15 %	70720	1.85E−03	3.50	2427	8164
			DGTD-$\mathbb{P}_3$:$\mathbb{P}_0$			
mesh-E	10 %	1560	5.65E−02	–	3	284
mesh-F	10 %	6640	1.50E−02	1.83	26	1048
mesh-G	9 %	27360	6.39E−03	1.20	441	4104
mesh-H	9 %	111040	1.76E−03	1.84	7271	16327
			DGTD-$\mathbb{P}_2$:$\mathbb{P}_1$			
mesh-E	36 %	1320	2.52E−02	–	2	142
mesh-F	35 %	5520	6.09E−03	1.98	11	524
mesh-G	34 %	22560	1.51E−03	1.98	184	2052
mesh-H	34 %	91200	3.79E−04	1.98	3016	8164
			DGTD-$\mathbb{P}_3$:$\mathbb{P}_1$			
mesh-E	26 %	1880	2.40E−02	–	3	284
mesh-F	24 %	7920	6.03E−03	1.92	31	1048
mesh-G	24 %	32480	1.51E−03	1.96	520	4104
mesh-H	23 %	131520	3.78E−04	1.98	8483	16327
			DGTD-$\mathbb{P}_3$:$\mathbb{P}_2$			
mesh-E	41 %	2360	2.03E−02	–	4	284
mesh-F	40 %	9840	4.96E−03	1.97	37	1048
mesh-G	38 %	40160	1.23E−03	1.99	621	4104
mesh-H	38 %	162240	3.06E−04	1.99	10041	16327
			DGTD-$\mathbb{P}_4$:$\mathbb{P}_2$			
mesh-E	31 %	3060	2.02E−02	–	5	354
mesh-F	30 %	12840	4.96E−03	1.96	58	1310
mesh-G	29 %	52560	1.23E−03	1.98	993	5130
mesh-H	29 %	212640	3.06E−04	1.99	16239	20409
			DGTD-$\mathbb{P}_4$:$\mathbb{P}_3$			
mesh-E	43 %	3700	2.03E−02	–	5	315
mesh-F	42 %	15400	4.96E−03	1.97	72	1310
mesh-G	42 %	62800	1.23E−03	1.99	1195	5130
mesh-H	40 %	253600	3.05E−04	2.00	20167	20409

[a] See Tab 3.8 for the characteristics of these meshes.
[b] Represents the percentage of the DOF in the fine mesh.

$$
\begin{aligned}
E_z &= J_\nu(\omega r)\sin(\nu\theta)\cos(\omega t),\\
H_x &= -\frac{y}{2r}[J_{\nu-1}(\omega r) - J_{\nu+1}(\omega r)]\sin(\nu\theta)\sin(\omega t)\\
&\quad -\frac{\nu x}{\omega r^2}J_\nu(\omega r)\cos(\nu\theta)\sin(\omega t),\\
H_y &= \frac{x}{2r}[J_{\nu-1}(\omega r) - J_{\nu+1}(\omega r)]\sin(\nu\theta)\sin(\omega t)\\
&\quad -\frac{\nu y}{\omega r^2}J_\nu(\omega r)\cos(\nu\theta)\sin(\omega t),
\end{aligned}
$$

where $\omega = 16.75883874736728$ and $\nu = \dfrac{14}{3}$ are obtained by enforcing the PEC condition on the boundaries. Numerical simulations make use of quasi-uniform triangular meshes with possibly obtuse angles (see Fig. 3.11 left). The percentage of triangles with obtuse angles is between 45 % and 50 % which correspond to a maximum angle between 94° and 91° respectively. The non-conforming meshes are obtained thanks to local refinements of a region situated between two arcs of the sector as shown on Fig. 3.11 right. Contour lines of the E_z component at times $t = 1$ and $t = 10$ are shown on Fig. 3.12 for a calculation based on the conforming DGTD-$\mathbb{P}_1$ method.

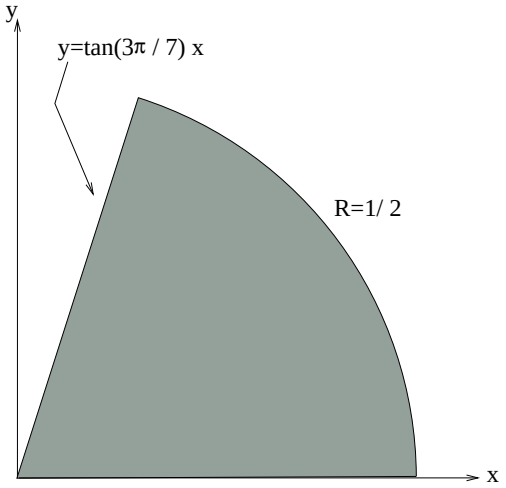

Figure 3.10: *Wedge-shaped PEC resonator setting.*

As for the previous test cases, we apply the h-refinement DGTD-$\mathbb{P}_p$ and hp-refinement DGTD-$\mathbb{P}_{p_c}$:$\mathbb{P}_{p_f}$ methods.

h-refinement DGTD-$\mathbb{P}_p$ method. For each polynomial degree p, we use four different conforming and non-conforming meshes whose characteristics are given in Tab. 3.13 and 3.14. The non-conforming meshes are obtained by locally refining (one refinement level) the zone of the domain bounded by the curves $\tan(9\pi/7\alpha) \leq y/x \leq \tan(3(\alpha-3)\pi/7\alpha)$ and $1/5 \leq x^2 + y^2 \leq 3/10$. The integer α takes a value in the set $\{9, 18, 36, 72\}$ depending on the mesh size. We summarize in Tab. 3.13 and 3.14 the L^2 error on E_z, the convergence rate, the CPU time and the number of time steps to reach $t = 0.75$. Fig. 3.13 shows the corresponding L^2 error on E_z as a function of the square root of the number of DOF. The observed numerical CFL values are given in Tab. 3.1. We can deduce from Tab. 3.13 and 3.14 that the DGTD-$\mathbb{P}_p$ method converges as $h^{(1)}$ if $p = 0$ and as $h^{(2)}$ if $p \geq 1$ (excepted for $p = 2$ using conforming meshes, where the convergence rate is close to $\mathcal{O}(h^{(2.5)})$).

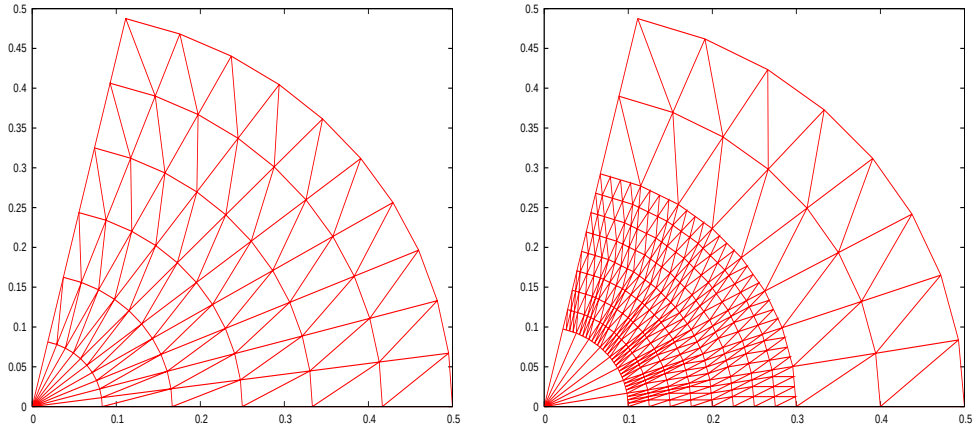

Figure 3.11: *Wedge-shaped PEC resonator.*
Example of conforming (left) and non-conforming (right) triangular meshes.

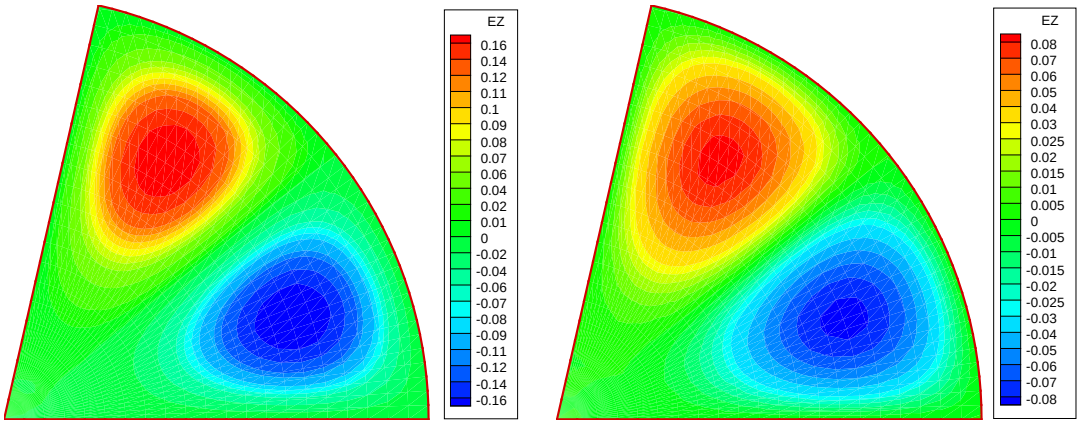

Figure 3.12: *Wedge-shaped PEC resonator.*
Contour lines of E_z *at* $t = 1$ *(left) and* $t = 10$ *(right).*
DGTD-$\mathbb{P}_1$ *method using a conforming mesh with* 862 *nodes and* 1640 *triangles.*

Tab. 3.13 and 3.14 and Fig.3.13 call for the following remarks:

- for this problem and using conforming meshes, it is clear that the gains in CPU time and memory usage are notable when the interpolation degree is increased. For example, to obtain an error level of 0.01%, the number of DOF required by the DGTD-$\mathbb{P}_1$, DGTD-$\mathbb{P}_2$ and DGTD-$\mathbb{P}_3$ methods is 16902, 5042 and 2500 respectively while the corresponding CPU times are 1700, 130 and 47 seconds (results not reported in a table below).
- using non-conforming meshes, it is not necessary to increase the interpolation degree to more than 2. For example, to achieve an error level of 0.01%, the number of DOF required by the DGTD-$\mathbb{P}_1$, DGTD-$\mathbb{P}_2$ and DGTD-$\mathbb{P}_3$ methods is 28560, 6402 and 10000 respectively while the corresponding CPU times are 2250, 160 and 420 seconds.
- the conforming h-refinement method is less expensive (in terms of the required number of DOF and CPU time) than the non-conforming one, however, the results obtained by using non-conforming meshes are very satisfactory despite of the presence of a large number of triangles in the refined zone.

Table 3.13: *Wedge-shaped PEC resonator. Convergence study for the h-refinement DGTD-$\mathbb{P}_p$ method using conforming meshes. L^2 error, CPU time and # time steps are measured at $t = 0.75$.*

Characteristics of the conforming meshes.						
# nodes	# triangles	# DOF	L^2 error	convergence rate	CPU (s)	# time steps
			DGTD-$\mathbb{P}_0$			
67	110	110	2.41E−02	–	$<< 1$	69
232	420	420	1.21E−02	1.03	2	247
862	1640	1640	6.22E−03	0.98	21	938
3322	6480	6480	3.16E−03	0.98	324	3656
			DGTD-$\mathbb{P}_1$			
67	110	330	5.06E−03	–	1	228
232	420	1260	1.36E−03	1.96	13	822
862	1640	4920	2.99E−04	2.22	169	3124
3322	6480	19440	7.98E−05	1.92	2780	12185
			DGTD-$\mathbb{P}_2$			
28	40	240	2.99E−03	–	1	139
86	144	864	8.47E−04	1.97	5	450
298	544	3264	1.70E−04	2.42	56	1608
1106	2112	12672	2.92E−05	2.59	838	6064
			DGTD-$\mathbb{P}_3$			
28	40	400	1.29E−03	–	2	277
86	144	1440	1.86E−04	3.02	15	899
298	544	5440	4.60E−05	2.10	190	3216
1106	2112	21120	1.16E−05	2.03	2807	12128

***hp*-refinement DGTD-$\mathbb{P}_{p_c}$:$\mathbb{P}_{p_f}$ method.** The numerical CFL values used are still those given in Tab. 3.9. The non-conforming meshes are those already used in conjunction with the h-refinement method. We summarize in Tab. 3.17 the L^2 error on E_z, the convergence rate, the CPU time and the number of time steps to reach $t = 0.75$. Fig. 3.14 shows the L^2 error on E_z as a function of the square root of the number of DOF. It can be seen from Tab. 3.17 that the DGTD-$\mathbb{P}_{p_c}$:$\mathbb{P}_{p_f}$ method converges as $h^{(2)}$, $\forall p_f \neq 0$ and for $p_f = 0$ the convergence rate is close to $\mathcal{O}(h^{(1.2)})$, $\forall p_c \neq 3$ (for $p_c = 3$ this rate is close to $\mathcal{O}(h^{(1)})$).

Table 3.14: *Wedge-shaped PEC resonator.*
Convergence study for the h-refinement DGTD-$\mathbb{P}_p$ method using non-conforming meshes.
L^2 errors, CPU times and # time steps are measured at $t = 0.75$.

Characteristics of the non-conforming meshes.							
# nodes	# hanging nodes	# triangles	# DOF	L^2 error	convergence rate	CPU (s)	# time steps
			DGTD-$\mathbb{P}_0$				
64	8	99	99	3.03E−02	–	<< 1	54
277	28	486	486	1.11E−02	1.26	2	202
1135	68	2124	2124	4.83E−03	1.13	22	804
4579	148	8856	8856	2.25E−03	1.07	398	3210
			DGTD-$\mathbb{P}_1$				
64	8	99	297	7.81E−03	–	2	179
277	28	486	1458	1.68E−03	1.93	12	673
1135	68	2124	6372	4.05E−04	1.93	192	2679
4579	148	8856	26568	8.08E−05	2.26	3329	10700
			DGTD-$\mathbb{P}_2$				
46	4	69 (mesh1[a])	414	1.92E−03	–	3	217
209	20	362 (mesh2)	2172	3.27E−04	2.14	19	789
871	52	1620 (mesh3)	9720	6.72E−05	2.11	328	3128
3539	116	6824 (mesh4)	40944	1.57E−05	2.03	5617	12487
			DGTD-$\mathbb{P}_3$				
46	4	69	690	1.03E−03	–	4	434
209	20	362	3620	2.43E−04	1.74	64	1577
871	52	1620	16200	6.29E−05	1.81	1125	6256
3539	116	6824	68240	1.53E−05	1.96	19067	24973

[a]This means that the mesh1 contains 46 nodes in which 4 are hanging nodes and 69 triangles, etc.

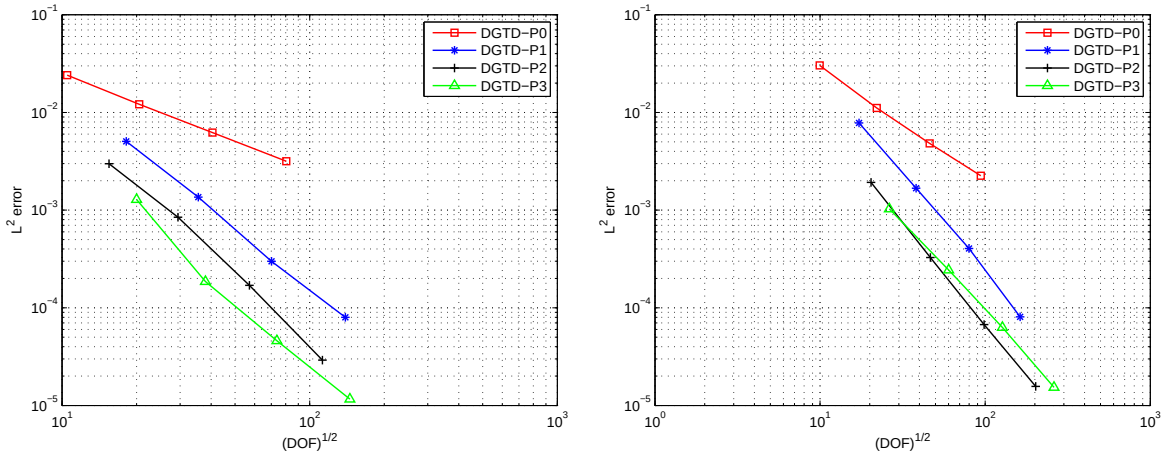

Figure 3.13: *Wedge-shaped PEC resonator.*
Numerical convergence of the h-refinement DGTD-$\mathbb{P}_p$ method.
Conforming (left) and non-conforming (right) triangular meshes.

Table 3.15: *Wedge-shaped PEC resonator.*
 # DOF and CPU time to reach an error level of 0.05%.
DGTD-$\mathbb{P}_{p_c}$:$\mathbb{P}_{p_f}$ method with locally refined meshes.

DGTD-$\mathbb{P}_{p_c}$:$\mathbb{P}_{p_f}$	$\mathbb{P}_1$:$\mathbb{P}_0$	$\mathbb{P}_2$:$\mathbb{P}_0$	$\mathbb{P}_2$:$\mathbb{P}_1$	$\mathbb{P}_3$:$\mathbb{P}_0$	$\mathbb{P}_3$:$\mathbb{P}_1$	$\mathbb{P}_3$:$\mathbb{P}_2$	$\mathbb{P}_4$:$\mathbb{P}_2$	$\mathbb{P}_4$:$\mathbb{P}_3$
# DOF	14502	22500	1296	57600	1530	1440	2010	2100
# CPU (s)	1600	2500	10	20000	19	15	25	27

Table 3.16: *Wedge-shaped PEC resonator.*
 # DOF and CPU time to reach an error level of 0.05%.
DGTD-$\mathbb{P}_p$ method using conforming meshes.

DGTD-$\mathbb{P}_p$	DGTD-$\mathbb{P}_1$	DGTD-$\mathbb{P}_2$	DGTD-$\mathbb{P}_3$
# DOF	3135	1308	760
# CPU (s)	70	12	6

A detailed analysis of Tab. 3.17 leads to the following remarks:

- it is not necessary to increase the polynomial degree in the coarse mesh to more than $p_c = p_f + 1$ (see Tab. 3.15). One can clearly deduce from Tab. 3.15 that the DGTD-$\mathbb{P}_2$:$\mathbb{P}_1$ method is the least expensive *hp*-refinement method for this problem.
- the DGTD-$\mathbb{P}_2$:$\mathbb{P}_1$ method is less expensive than the non-conforming DGTD-$\mathbb{P}_p$ methods. For example, we have observed (results not reported in a table here) that to obtain an error level of 0.05%, on one hand, the DGTD-$\mathbb{P}_1$ and DGTD-$\mathbb{P}_2$ methods require 5184 and 1482 DOF respectively while the corresponding CPU times are 130 and 13 seconds and, on the other hand, the DGTD-$\mathbb{P}_2$:$\mathbb{P}_1$ method needs 1296 DOF and 10 seconds (see Tab. 3.15).
- the DGTD-$\mathbb{P}_2$:$\mathbb{P}_1$ method can be compared with the conforming DGTD-$\mathbb{P}_p$ one. Indeed, the results of Tab. 3.15 together with those of Tab. 3.16 show that the DGTD-$\mathbb{P}_2$:$\mathbb{P}_1$ method is less expensive than the DGTD-$\mathbb{P}_1$ and DGTD-$\mathbb{P}_2$ methods, but it is not much more expensive than the DGTD-$\mathbb{P}_3$ method. One can note here that the results of the DGTD-$\mathbb{P}_2$:$\mathbb{P}_1$ method remain very satisfactory despite that the space $\mathbb{P}_1$ is used in 38% of the triangles of the mesh.

4 Heterogeneous media

This section is devoted to the numerical evaluation of the conforming and non-conforming DGTD methods in the context of wave propagation problems in heterogeneous media. As in the previous section, we have selected test cases for which analytical solution are available:

1. a rectangular PEC resonator with one material interface,
2. a dielectric in a PEC cavity with two material interfaces,
3. a dielectric cylinder illuminated by a plane wave.

4.1 Rectangular PEC resonator with one material interface

We consider a problem in which a dielectric of relative permittivity ϵ_2 occupying the spatial region $[0, 0.5] \times [0, 1]$, is enclosed by PEC-bounded $[0, 1.25] \times [0, 1]$ domain. The exact time-domain solution is [41]:

Table 3.17: *Wedge-shaped PEC resonator. Convergence study of the DGTD-$\mathbb{P}_{p_c}$:$\mathbb{P}_{p_f}$ method. Non-conforming locally refined meshes. L^2 error, CPU time and # time steps are measured at $t = 0.75$.*

mesh[a]	% DOF$_f$[b]	# DOF	L^2 error	convergence rate	CPU (s)	# time steps
			DGTD-$\mathbb{P}_1$:$\mathbb{P}_0$			
mesh1	4%	191	9.76E−03	–	1	145
mesh2	15%	830	2.52E−03	1.84	6	526
mesh3	20%	3452	1.23E−03	1.00	81	2086
mesh4	23%	14072	5.28E−04	1.21	1426	8325
			DGTD-$\mathbb{P}_2$:$\mathbb{P}_0$			
mesh1	2%	374	4.68E−03	–	2	217
mesh2	8%	1532	2.07E−03	1.16	15	789
mesh3	11%	6200	1.02E−03	1.00	210	3128
mesh4	13%	24944	4.45E−04	1.20	3544	12487
			DGTD-$\mathbb{P}_3$:$\mathbb{P}_0$			
mesh1	1%	618	3.99E−03	–	4	434
mesh2	5%	2468	2.05E−03	0.97	44	1577
mesh3	7%	9864	1.06E−03	0.95	675	6256
mesh4	8%	39440	6.01E−04	0.82	11159	24973
			DGTD-$\mathbb{P}_2$:$\mathbb{P}_1$			
mesh1	6%	390	1.96E−03	–	2	217
mesh2	21%	1788	3.58E−04	2.23	16	789
mesh3	28%	7608	8.28E−05	2.02	258	3128
mesh4	31%	31344	1.90E−05	2.08	4415	12487
			DGTD-$\mathbb{P}_3$:$\mathbb{P}_1$			
mesh1	4%	634	1.19E−03	–	5	434
mesh2	14%	2724	2.71E−04	2.03	47	1577
mesh3	19%	11272	7.22E−05	1.86	771	6256
mesh4	21%	45840	1.73E−05	2.04	12836	24973
			DGTD-$\mathbb{P}_3$:$\mathbb{P}_2$			
mesh1	7%	658	1.03E−03	–	4	434
mesh2	25%	3108	2.42E−04	1.86	53	1577
mesh3	32%	13384	6.25E−05	1.86	913	6256
mesh4	35%	55440	1.46E−05	2.04	15583	24973
			DGTD-$\mathbb{P}_4$:$\mathbb{P}_2$			
mesh1	5%	963	1.00E−03	–	7	542
mesh2	18%	4278	2.47E−04	1.88	92	1971
mesh3	24%	17964	6.18E−05	1.93	1555	7820
mesh4	26%	73560	1.46E−05	2.05	25687	31250
			DGTD-$\mathbb{P}_4$:$\mathbb{P}_3$			
mesh1	8%	995	1.01E−03	–	7	542
mesh2	27%	4790	2.46E−04	1.80	103	1971
mesh3	34%	20780	6.16E−05	1.89	1763	7820
mesh4	37%	86360	1.45E−05	2.03	30003	31250

[a] See Tab. 3.14 for the characteristics of the meshes.
[b] Represents the percentage of the DOF in the fine mesh.

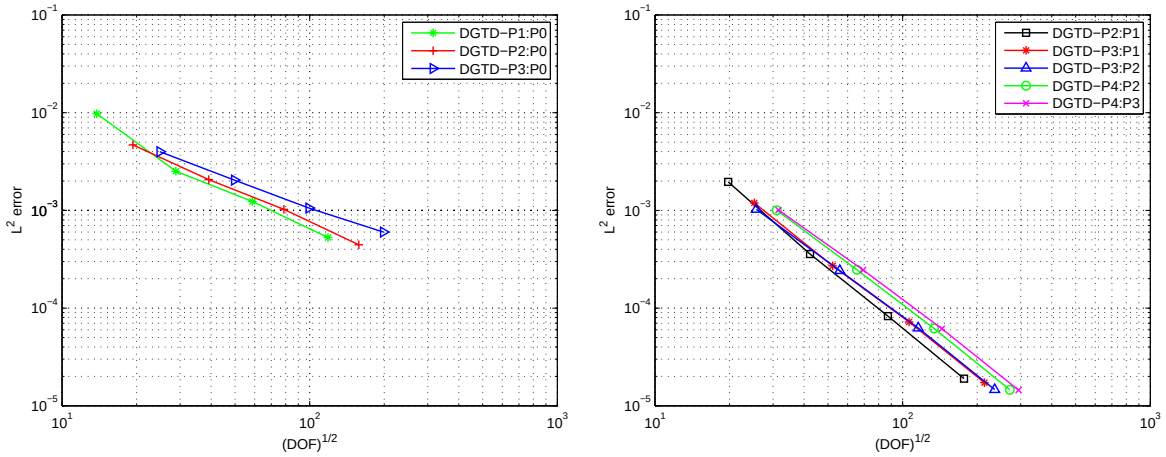

Figure 3.14: *Wedge-shaped PEC resonator.*
Numerical convergence of the hp-refinement DGTD-$\mathbb{P}_{p_c}$.$\mathbb{P}_{p_f}$ method.
Non-conforming triangular meshes.

$$E_z = \begin{cases} \sin(a_1 x)\sin(\omega t)\sin(by), & 0 \le x \le \frac{1}{2}, \quad 0 \le y \le 1, \\ \cos(a_2 x)\sin(\omega t)\sin(by), & \frac{1}{2} \le x \le \frac{5}{4}, \quad 0 \le y \le 1, \end{cases}$$

$$H_x = \begin{cases} \frac{b}{\omega}\sin(a_1 x)\cos(\omega t)\cos(by), & 0 \le x \le \frac{1}{2}, \quad 0 \le y \le 1, \\ \frac{b}{\omega}\cos(a_2 x)\cos(\omega t)\cos(by), & \frac{1}{2} \le x \le \frac{5}{4}, \quad 0 \le y \le 1, \end{cases}$$

$$H_y = \begin{cases} -\frac{a_1}{\omega}\cos(a_1 x)\cos(\omega t)\sin(by), & 0 \le x \le \frac{1}{2}, \quad 0 \le y \le 1, \\ \frac{a_2}{\omega}\sin(a_2 x)\cos(\omega t)\sin(by), & \frac{1}{2} \le x \le \frac{5}{4}, \quad 0 \le y \le 1, \end{cases}$$

where $a_1^2 + b^2 = \epsilon_2\omega^2$, $a_2^2 + b^2 = \epsilon_1\omega^2$, $\sin(\frac{a_1}{2}) = \cos(\frac{a_2}{2})$ and $\cos(\frac{5a_2}{4}) = 0$. The values of the parameters appearing in these relations are defined by imposing the PEC condition on the boundary $x = 5/4$ and by ensuring the continuity of E_z across the material interface $x = 1/2$. As in [41]-[40], these parameter values are chosen as $\epsilon_1 = 1$, $\epsilon_2 = 2$, $a_1 = 3\pi$, $a_2 = 2\pi$, $b = \pi$, and $\omega = \sqrt{5}\pi$. The wavelength is $\lambda^{\epsilon_1} = 0.268$ in the air zone and $\lambda^{\epsilon_2} = 0.189$ in the dielectric zone, *i.e.* $\lambda^{\epsilon_1} \simeq 1.42\lambda^{\epsilon_2}$. Across the dielectric interface (*i.e.* the air/dielectric interface), the tangential components of the electromagnetic field E_z and H_y are continuous as well their first y derivative. Furthermore, the first x derivative of E_z is continuous while that of H_y is discontinuous. An example plot of analytical solution is shown on Fig. 4.1.

Numerical simulations make use of uniform triangular meshes such that the material interface $x = 1/2$ is aligned with the grid, *i.e.* the intersection between the interface $x = 1/2$ and int(T_i) (the interior of T_i) is empty, $\forall$ triangle T_i of the mesh (see Fig. 4.2 left). Hence, the mesh shown on Fig. 4.2 right is not allowed in the present modeling. One can note here that some FDTD schemes may not need this condition on the material interface [41]. Contour lines of the E_z component at times $t = 1$ and $t = 10$ are shown on Fig. 4.3 for a calculation based on the conforming DGTD-$\mathbb{P}_1$ method.

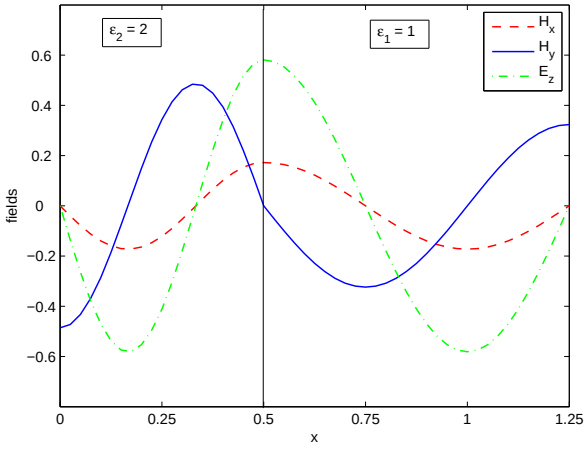

Figure 4.1: *Rectangular PEC resonator with one material interface. Plots of the analytical solution along the line $y = 3/4$ at time $t = 0.75$.*

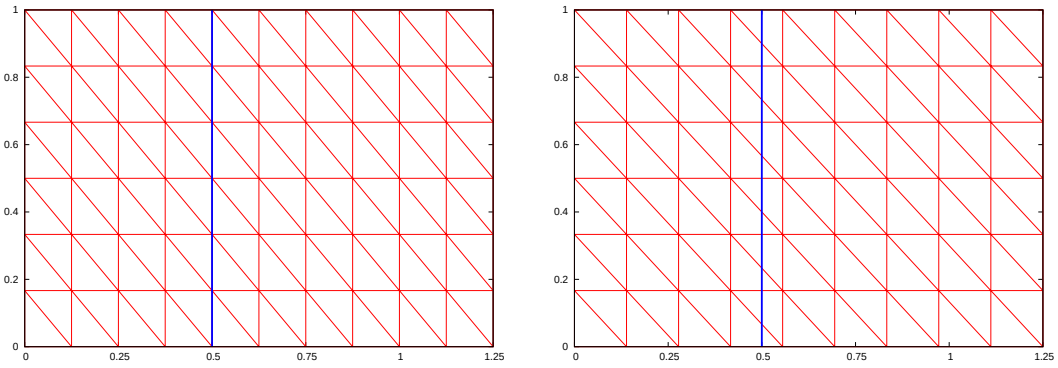

Figure 4.2: *Rectangular PEC resonator with one material interface. Example of two possible configurations of a conforming triangular mesh. The left figure shows the mesh used in the present study and the right figure shows a situation of mesh wich is not allowed in our modeling. The blue line represents the material interface.*

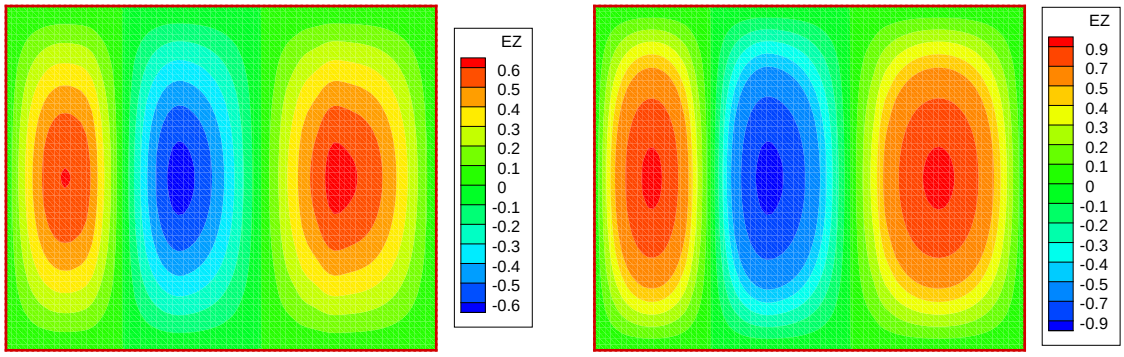

Figure 4.3: *Rectangular PEC resonator with one material interface. Contour lines of* E_z *at* $t = 1$ *(left) and* $t = 10$ *(right). DGTD-*$\mathbb{P}_1$ *method using a conforming mesh with* 4941 *nodes and* 9600 *triangles.*

h-refinement DGTD-$\mathbb{P}_p$ method. The non-conforming meshes are obtained by locally refining (one refinement level) the material region *i.e.* the zone $[0, 0.5] \times [0, 1]$. Tab. 4.1 and 4.2 give the L^2 error on E_z and $(\mathbf{E}, \mathbf{H}) = (E_z, H_x, H_y)$, the convergence rate, the CPU time and the number of time steps to reach $t = 1$ using conforming and non-conforming meshes. Fig. 4.4 shows the corresponding L^2 error on the electromagnetic field $(\mathbf{E}, \mathbf{H})$ as a function of the square root of the number of DOF. The numerical CFL values used here are given in Tab. 3.1. We can deduce from these results that the convergence rate of the DGTD-$\mathbb{P}_p$ method is close to $\mathcal{O}(h^{(1)})$, $\forall p$. Moreover, it is not necessary to increase the interpolation degree p to more than one since doing so does not result in a higher convergence rate and the method becomes too much expensive for $p \geq 2$ (see Tab. 4.5). It is clear that the presence of a material interface influences the convergence rate of the DGTD-$\mathbb{P}_p$ method but this behaviour does not depend on the type of material. We validate this by studying the convergence of the conforming DGTD-$\mathbb{P}_p$ method using three different materials. Results in Tab. 4.3 show that the convergence rate is always close to $\mathcal{O}(h^{(1)})$. This confirms that the convergence rate depends only on the regularity of the solution. It is expected that the use of different locations of material interfaces would make the situation worse. This phenomenon has been observed in [21] and in the more recent work [5] for the Maxwell eigenvalue problem (see Remark 1). This is also observed in [14] for the time-harmonic Maxwell equations using high order continuous and discontinuous Galerkin methods.

Remark 1 *In [5] a checkerboard pattern of materials inside a PEC cavity is studied using a high order discontinuous Galerkin method. It is observed that the convergence rate is less than linear, whatever the interpolation degree is, despite that without material interfaces (*i.e. *in homogeneous media) the convergence rate is close to* $\mathcal{O}(h^{(2p)})$*. The authors in [5] do not elaborate on this fact. Moreover, this problem was also studied in [21] using high order nodal h- and p-refinement discontinuous Galerkin method with central fluxes. As in [5], the convergence of the nodal discontinuous Galerkin method turned sour in the presence of material interfaces. According to the authors of [21] the degradation of the convergence is due to the use of centered fluxes at the material interfaces (or at discontinuities). The authors indicate that by defining material properties at material interfaces as the average of cell values (*i.e. *by using a* regularization technique *[34]) should improve the situation.*

Table 4.1: *Rectangular PEC resonator with one material interface. Convergence study for the h-refinement DGTD-$\mathbb{P}_p$ method using conforming meshes. L^2 error, CPU time and # time steps are measured at $t = 1$.*

# DOF	error on E_z	convergence rate on E_z	error on (**E**,**H**)	convergence rate on (**E**,**H**)	CPU (s)	# time steps
			DGTD-$\mathbb{P}_0$			
4000	1.40E−02	–	3.26E−02	–	1	57
16000	6.73E−03	1.06	1.91E−02	0.77	10	114
64000	3.33E−03	1.02	9.06E−03	1.08	79	227
256000	1.66E−03	1.01	4.11E−03	1.14	644	453
			DGTD-$\mathbb{P}_1$			
12000	5.30E−02	–	7.18E−02	–	8	189
48000	2.72E−02	0.96	3.63E−02	0.98	58	378
192000	1.38E−02	0.99	1.86E−02	0.97	483	755
768000	6.91E−03	0.99	9.51E−03	0.97	3861	1509
			DGTD-$\mathbb{P}_2$			
14400	6.88E−02	–	9.21E−02	–	9	220
57600	3.47E−02	0.99	4.76E−02	0.95	65	439
230400	1.74E−02	1.00	2.37E−02	1.01	535	878
921600	8.68E−03	1.00	1.20E−02	0.98	4503	1755
			DGTD-$\mathbb{P}_3$			
24000	6.89E−02	–	9.38E−02	–	27	439
96000	3.47E−02	0.99	4.76E−02	0.98	220	878
384000	1.74E−02	1.00	2.41E−02	0.98	1837	1755
1536000	8.68E−03	1.00	1.20E−02	1.01	14917	3510

Table 4.2: *Rectangular PEC resonator with one material interface. Convergence study for the h-refinement DGTD-$\mathbb{P}_p$ method using non-conforming meshes. L^2 error, CPU time and # time steps are measured at $t = 1$.*

# DOF	error on E_z	convergence rate on E_z	error on (**E**,**H**)	convergence rate on (**E**,**H**)	CPU (s)	# time steps
			DGTD-$\mathbb{P}_0$			
5280	1.02E−02	–	2.02E−02	–	2	88
21120	4.93E−03	1.05	1.09E−02	0.88	21	176
84480	2.45E−03	1.01	5.15E−03	1.09	166	351
337920	1.22E−03	1.00	2.74E−03	0.91	1350	702
			DGTD-$\mathbb{P}_1$			
15840	6.71E−02	–	9.06E−02	–	15	293
63360	3.43E−02	0.97	4.76E−02	0.93	122	585
253440	1.73E−02	0.99	2.41E−02	0.98	1004	1170
1013760	8.66E−03	1.00	1.20E−02	1.00	8272	2340
			DGTD-$\mathbb{P}_2$			
9900	1.08E−01	–	1.46E−01	–	7	250
39600	5.54E−02	0.96	7.63E−02	0.94	51	500
158400	2.78E−02	0.99	3.88E−02	0.96	425	1000
633600	1.39E−02	1.00	1.95E−02	0.99	3462	2000
			DGTD-$\mathbb{P}_3$			
16500	1.08E−01	–	1.46E−01	–	20	500
66000	5.54E−02	0.96	7.62E−02	0.94	172	1000
264000	2.78E−02	0.99	3.88E−02	0.98	1410	2000
1056000	1.39E−02	1.00	1.95E−02	0.99	12051	4000

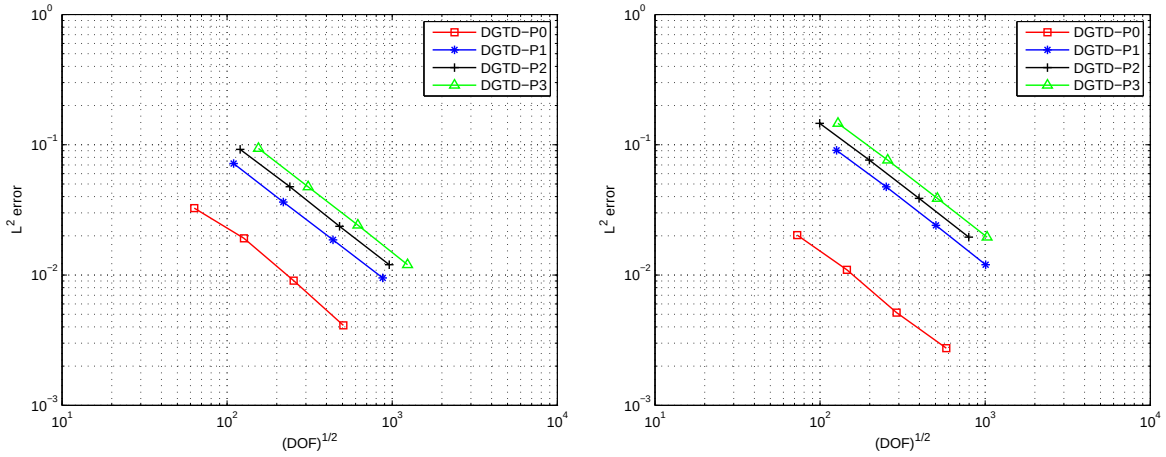

Figure 4.4: *Rectangular PEC resonator with one material interface. Numerical convergence of the h-refinement DGTD-$\mathbb{P}_p$ method. Conforming (left) and non-conforming (right) triangular meshes.*

Table 4.3: *Rectangular PEC resonator with one material interface for different types of materials. Convergence study for the DGTD-$\mathbb{P}_p$ method using conforming meshes. L^2 error, CPU time and # time steps are measured at $t = 1$.*

	$\epsilon_2 = 2.125$ $\omega = \sqrt{40}\pi$		$\epsilon_2 = 3.25$ $\omega = \sqrt{20}\pi$		$\epsilon_2 = 6.625$ $\omega = \sqrt{8}\pi$	
# DOF	error on (**E**,**H**)	convergence rate on (**E**,**H**)	error on (**E**,**H**)	convergence rate on (**E**,**H**)	error on (**E**,**H**)	convergence rate on (**E**,**H**)
	DGTD-$\mathbb{P}_0$		DGTD-$\mathbb{P}_0$		DGTD-$\mathbb{P}_0$	
4000	1.06E−01	–	1.28E−01	–	1.90E−01	–
16000	5.41E−02	0.97	6.41E−02	1.00	9.25E−02	1.04
64000	2.66E−02	1.02	3.20E−02	1.00	4.63E−02	1.00
256000	1.19E−02	1.15	1.51E−02	1.08	2.30E−02	1.00
	DGTD-$\mathbb{P}_1$		DGTD-$\mathbb{P}_1$		DGTD-$\mathbb{P}_1$	
12000	2.21E−01	–	2.72E−01	–	3.86E−01	–
48000	1.23E−01	0.84	1.48E−01	0.87	2.07E−01	0.90
192000	6.62E−02	0.90	7.87E−02	0.92	1.06E−01	0.96
768000	3.47E−02	0.93	4.09E−02	0.94	5.39E−02	0.98
	DGTD-$\mathbb{P}_2$		DGTD-$\mathbb{P}_2$		DGTD-$\mathbb{P}_2$	
14400	3.45E−01	–	3.84E−01	–	4.44E−01	–
57600	1.78E−01	0.95	2.03E−01	0.92	2.38E−01	0.90
230400	8.87E−02	1.01	1.01E−01	1.01	1.21E−01	0.97
921600	4.49E−02	0.98	5.13E−02	0.98	6.12E−02	0.98
	DGTD-$\mathbb{P}_3$		DGTD-$\mathbb{P}_3$		DGTD-$\mathbb{P}_3$	
24000	3.46E−01	–	3.93E−01	–	4.47E−01	–
96000	1.79E−01	0.96	2.03E−01	0.95	2.38E−01	0.91
384000	8.87E−02	1.01	1.03E−01	0.98	1.21E−01	0.97
1536000	4.49E−02	0.98	5.15E−02	1.00	6.12E−02	0.98

***hp*-refinement DGTD-$\mathbb{P}_{p_c}$:$\mathbb{P}_{p_f}$ method.** Here the non-conforming meshes are obtained by locally refining (one refinement level) the zone $[0, 0.55] \times [0, 1]$. Tab. 4.6 gives the L^2 error on E_z and $(\mathbf{E}, \mathbf{H}) = (E_z, H_x, H_y)$, the convergence rate, the CPU time and the number of time steps to reach $t = 1$. Fig. 4.5 shows the corresponding L^2 error on $(\mathbf{E}, \mathbf{H})$ as a function of the square root of the number of DOF. The numerical CFL values are given in Tab. 4.4. It is found from Tab. 4.6 that the convergence rate of the DGTD-$\mathbb{P}_{p_c}$:$\mathbb{P}_{p_f}$ method is close to $\mathcal{O}(h^{(1)})$, $\forall p_c, p_f$. One can also note that to obtain a given error level the DGTD-$\mathbb{P}_1$:$\mathbb{P}_0$ is the least expensive of all *hp*-refinement and *h*-refinement methods (see Tab. 4.5).

Table 4.4: *Rectangular PEC resonator with one material interface. Numerical CFL conditions for the DGTD-$\mathbb{P}_{p_c}$:$\mathbb{P}_{p_f}$ method.*

$p_c : p_f$	1 : 0	2 : 0	3 : 0	2 : 1	3 : 1	3 : 2
CFL	0.7	0.4	0.25	0.3	0.25	0.2

Table 4.5: *Rectangular PEC resonator with one material interface. # DOF and CPU time to reach an error level of 2% on the electromagnetic field (**E**,**H**). DGTD-$\mathbb{P}_{p_c}$:$\mathbb{P}_{p_f}$ and DGTD-$\mathbb{P}_p$ methods.*

DGTD-$\mathbb{P}_{p_c}$:$\mathbb{P}_{p_f}$	$\mathbb{P}_1$:$\mathbb{P}_0$	$\mathbb{P}_2$:$\mathbb{P}_0$	$\mathbb{P}_3$:$\mathbb{P}_0$	$\mathbb{P}_2$:$\mathbb{P}_1$	$\mathbb{P}_3$:$\mathbb{P}_1$	$\mathbb{P}_3$:$\mathbb{P}_2$
# DOF	4092	7750	6990	93024	122500	184920
CPU (s)	2	5	5	185	290	485

DGTD-$\mathbb{P}_p$ on conforming meshes.	$\mathbb{P}_0$	$\mathbb{P}_1$	$\mathbb{P}_2$	$\mathbb{P}_3$
# DOF	14161	164025	324900	562500
CPU (s)	8	380	900	3150

DGTD-$\mathbb{P}_p$ on non-conforming meshes.	$\mathbb{P}_0$	$\mathbb{P}_1$	$\mathbb{P}_2$	$\mathbb{P}_3$
# DOF	5280	360000	592800	1000000
CPU (s)	2	1730	3120	10800

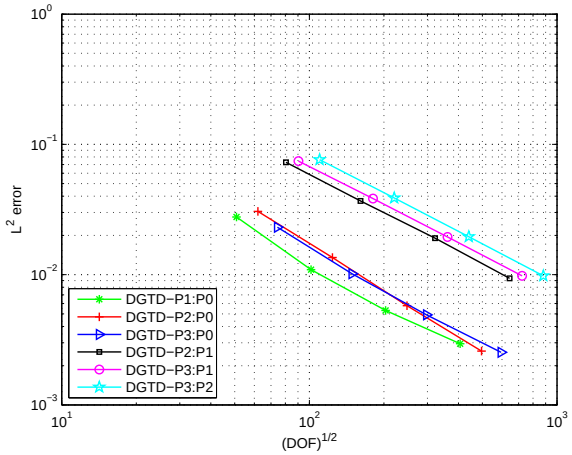

Figure 4.5: *Rectangular PEC resonator with one material interface. Numerical convergence of the hp-refinement DGTD-$\mathbb{P}_{p_c}$:$\mathbb{P}_{p_f}$ method. Non-conforming triangular meshes.*

Table 4.6: *Rectangular PEC resonator with one material interface. Convergence study of the DGTD-$\mathbb{P}_{p_c}$:$\mathbb{P}_{p_f}$ method. Non-conforming locally refined meshes. L^2 error, CPU time and # time steps are measured at $t = 1$.*

# DOF	error on **E**	convergence rate on **E**	error on (**E**,**H**)	convergence rate on (**E**,**H**)	CPU (s)	# time steps
			DGTD-$\mathbb{P}_1$:$\mathbb{P}_0$			
2580	1.29E−02	–	2.77E−02	–	1	72
10320	5.08E−03	1.35	1.09E−02	1.34	6	143
41280	2.24E−03	1.18	5.31E−03	1.04	52	286
165120	1.06E−03	1.07	2.95E−03	0.85	429	572
			DGTD-$\mathbb{P}_2$:$\mathbb{P}_0$			
3840	1.82E−02	–	3.06E−02	–	2	125
15360	8.86E−03	1.04	1.35E−02	1.18	14	250
61440	3.58E−03	1.30	5.77E−03	1.23	115	500
245760	1.38E−03	1.37	2.59E−03	1.16	928	1000
			DGTD-$\mathbb{P}_3$:$\mathbb{P}_0$			
5520	1.18E−02	–	2.31E−02	–	4	200
22080	4.83E−03	1.29	1.02E−02	1.19	28	400
88320	2.21E−03	1.13	4.92E−03	1.05	232	800
353280	1.06E−03	1.06	2.53E−03	0.96	1895	1600
			DGTD-$\mathbb{P}_2$:$\mathbb{P}_1$			
6480	5.36E−02	–	7.28E−02	–	3	167
25920	2.74E−02	0.97	3.68E−02	0.99	25	334
103680	1.38E−02	0.99	1.90E−02	0.95	214	667
414720	6.92E−03	1.00	9.37E−03	1.02	1792	1334
			DGTD-$\mathbb{P}_3$:$\mathbb{P}_1$			
8160	5.36E−02	–	7.43E−02	–	4	200
32640	2.74E−02	0.97	3.84E−02	0.95	40	400
130560	1.38E−02	0.99	1.95E−02	0.98	317	800
522240	6.92E−03	1.00	9.79E−03	0.99	2537	1600
			DGTD-$\mathbb{P}_3$:$\mathbb{P}_2$			
12120	5.53E−02	–	7.63E−02	–	7	250
48480	2.78E−02	0.99	3.88E−02	0.98	63	500
193920	1.39E−02	1.00	1.95E−02	0.99	523	1000
775680	6.94E−03	1.00	9.79E−03	1.00	4270	2000

4.2 Dielectric in a PEC cavity with two material interfaces

In this problem, a lossless dielectric with a relative permittivity ϵ_2 is enclosed by air in the x direction. The media are nonmagnetic, and homogeneuous along y direction. The computational domain $\Omega = [-1,1]\times[-1,1]$ is bounded by PEC walls. The permittivity is given as $\epsilon = \epsilon_1$ if $\frac{1}{2} \leq |x| \leq 1$ and $|y| \leq 1$, and $\epsilon = \epsilon_2$ if $|x| \leq \frac{1}{2}$ and $|y| \leq 1$, where $\epsilon_1 = 1$ and $\epsilon_2 = 2.25$. The exact time-domain solution is [41]:

$$E_z = \begin{cases} \sin(\frac{\omega_2}{2})\sin(\omega_1(x+1))\sin(\omega_y y)\cos(\omega t), & -1 \leq x < -\frac{1}{2}, \quad |y| \leq 1, \\ -\sin(\frac{\omega_1}{2})\sin(\omega_2 x)\sin(\omega_y y)\cos(\omega t), & -\frac{1}{2} \leq x \leq \frac{1}{2}, \quad |y| \leq 1, \\ \sin(\frac{\omega_2}{2})\sin(\omega_1(x-1))\sin(\omega_y y)\cos(\omega t), & \frac{1}{2} \leq x \leq 1, \quad |y| \leq 1, \end{cases}$$

$$H_x = \begin{cases} -\frac{\omega_y}{\omega}\sin(\frac{\omega_2}{2})\sin(\omega_1(x+1))\cos(\omega_y y)\sin(\omega t), & -1 \leq x < -\frac{1}{2}, \quad |y| \leq 1, \\ \frac{\omega_y}{\omega}\sin(\frac{\omega_1}{2})\sin(\omega_2 x)\cos(\omega_y y)\sin(\omega t), & -\frac{1}{2} \leq x \leq \frac{1}{2}, \quad |y| \leq 1, \\ -\frac{\omega_y}{\omega}\sin(\frac{\omega_2}{2})\sin(\omega_1(x-1))\cos(\omega_y y)\sin(\omega t), & \frac{1}{2} \leq x \leq 1, \quad |y| \leq 1, \end{cases}$$

$$H_y = \begin{cases} \frac{\omega_1}{\omega}\sin(\frac{\omega_2}{2})\cos(\omega_1(x+1))\sin(\omega_y y)\sin(\omega t), & -1 \leq x < -\frac{1}{2}, \quad |y| \leq 1, \\ -\frac{\omega_2}{\omega}\sin(\frac{\omega_1}{2})\cos(\omega_2 x)\sin(\omega_y y)\sin(\omega t), & -\frac{1}{2} \leq x \leq \frac{1}{2}, \quad |y| \leq 1, \\ \frac{\omega_1}{\omega}\sin(\frac{\omega_2}{2})\cos(\omega_1(x-1))\sin(\omega_y y)\sin(\omega t), & \frac{1}{2} \leq x \leq 1, \quad |y| \leq 1, \end{cases}$$

where $\omega_1^2 + \omega_y^2 = \epsilon_1\omega^2$ and $\omega_2^2 + \omega_y^2 = \epsilon_2\omega^2$. The value of ω_y is determined according to the relation:

$$\sqrt{\epsilon_2\omega^2 - \omega_y^2}\tan\left(\frac{\sqrt{\epsilon_1\omega^2 - \omega_y^2}}{2}\right) = \sqrt{\epsilon_1\omega^2 - \omega_y^2}\tan\left(-\frac{\sqrt{\epsilon_2\omega^2 - \omega_y^2}}{2}\right).$$

As in [41] we choose $\omega_y = 2\pi$ to satisfy the PEC conditions on $y = \pm 1$ wich leads to $\omega = 9.07716175885174$. The wavelength $\lambda^{\epsilon_1} = 0.208$ in the air zone and $\lambda^{\epsilon_2} = 0.138$ in the material region, *i.e.* $\lambda^{\epsilon_1} \simeq 1.5\lambda^{\epsilon_2}$. Note that across the dielectric interface (*i.e.* at $x = \pm 1/2$), the E_z and H_x components, their time derivative and their first y derivative are continuous while their first x derivative are discontinuous. Furthermore, the H_y component and all its derivatives are discontinuous. An example plot of the analytical solution is shown on Fig. 4.6. Contour lines of the H_y and E_z components at times $t = 1$ and $t = 10$ are shown on Fig. 4.7 for a calculation based on the conforming DGTD-$\mathbb{P}_1$ method.

h-refinement DGTD-$\mathbb{P}_p$ method. The non-conforming meshes are obtained by locally refining (one refinement level) the material region *i.e.* the zone $[-0.5, 0.5]\times[-1,1]$. Tab. 4.8 and 4.9 give the L^2 error on E_z, H_y and $(\mathbf{E},\mathbf{H})$, the convergence rate, the CPU time and the number of time steps to reach $t = 0.65$ using conforming and non-conforming meshes. Fig. 4.8 shows the corresponding L^2 error on $(\mathbf{E},\mathbf{H})$ as a function of the square root of the number of DOF. The convergence rate of the DGTD-$\mathbb{P}_p$ method is close to $\mathcal{O}(h^{(1)})$ for $p = 0, 1$, and close to $\mathcal{O}(h^{(1/3)})$ for $p = 2, 3$.

hp-refinement DGTD-$\mathbb{P}_{p_c}$:$\mathbb{P}_{p_f}$ method. Similarly to the h-refinement method, the non-conforming meshes are obtained by locally refining (one refinement level) the region $[-0.5, 0.5]\times[-1,1]$. Tab. 4.10

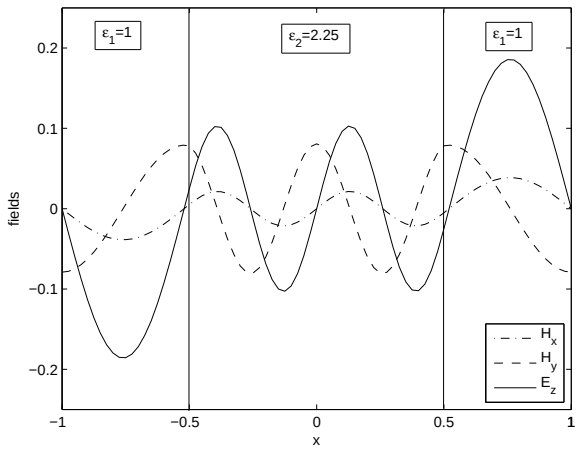

Figure 4.6: *Dielectric in a PEC cavity with two material interfaces. Plots of the analytical solution along the line* $y = \dfrac{1}{3}$ *at time* $t = 0.75$.

gives the L^2 error on E_z, H_y and $(\mathbf{E}, \mathbf{H})$, the convergence rate, the CPU time and the number of time steps to reach $t = 0.65$. Fig. 4.9 shows the corresponding L^2 error on $(\mathbf{E}, \mathbf{H})$ as a function of the square root of the number of DOF. The numerical CFL values are given in Tab. 4.4. It can be seen from Tab. 4.10 that the overall convergence rate of the DGTD-$\mathbb{P}_{p_c}$:$\mathbb{P}_{p_f}$ is close to $\mathcal{O}(h^{(1)})$, excepted for the DGTD-$\mathbb{P}_3$:$\mathbb{P}_2$ method for which the convergence rate is close to $\mathcal{O}(h^{(1/3)})$.

Despite the slow convergence rate of the DGTD-$\mathbb{P}_p$ (for $p \geq 2$) and DGTD-$\mathbb{P}_{p_c}$:$\mathbb{P}_{p_f}$ (for $p_c \geq 3,\ p_f \geq 2$) methods, the role of the high order DGTD method remains very important to reduce the numerical dispersion even in the presence of material interfaces. To illustrate this point, we plot on Fig 4.10 and 4.11 the time evolution of the L^2 error on the electromagnetic field (**E**,**H**) for calculations based on the DGTD-$\mathbb{P}_p$ and DGTD-$\mathbb{P}_{p_c}$:$\mathbb{P}_{p_f}$ methods using conforming and non-conforming meshes with 6 and 4 points per λ^{ϵ_1} respectively.

Next, we study the numerical convergence of the DGTD-$\mathbb{P}_p$ method for different materials and using conforming meshes. In Tab 4.7 we summarize the relative permettivity $\epsilon_r = \epsilon_2$ for several materials. Our objective here, is to understand the influence of the material type on the convergence rate. We give in Tab 4.11 and 4.12 the L^2 error on the E_z component and the corresponding convergence rate for some materials. We can conclude that:

- the DGTD-$\mathbb{P}_0$ method converges as $h^{(1)}$ in the heterogeneuous and homogeneuous cases.
- in the homogeneuous case, the DGTD-$\mathbb{P}_1$ converges as $h^{(2)}$, but the convergence rate is reduced to $\mathcal{O}(h^{(1)})$ in the heterogeneous case.
- for $p \geq 2$, the DGTD-$\mathbb{P}_p$ methods converge as $h^{(2)}$ in the homogeneous case. This convergence rate is reduced to $\mathcal{O}(h^{(1)})$ or less than linear in the heterogeneous case.

4.3 Scattering of a dielectric cylinder

We consider now a typical problem, in which a plane wave impinges on a dielectric cylinder, experiencing reflection and refraction at the material interface. The geometry of the scenario is shown in Fig. 4.12.

We assume that the cylinder is illuminated by a monochromatic plane wave of the form:

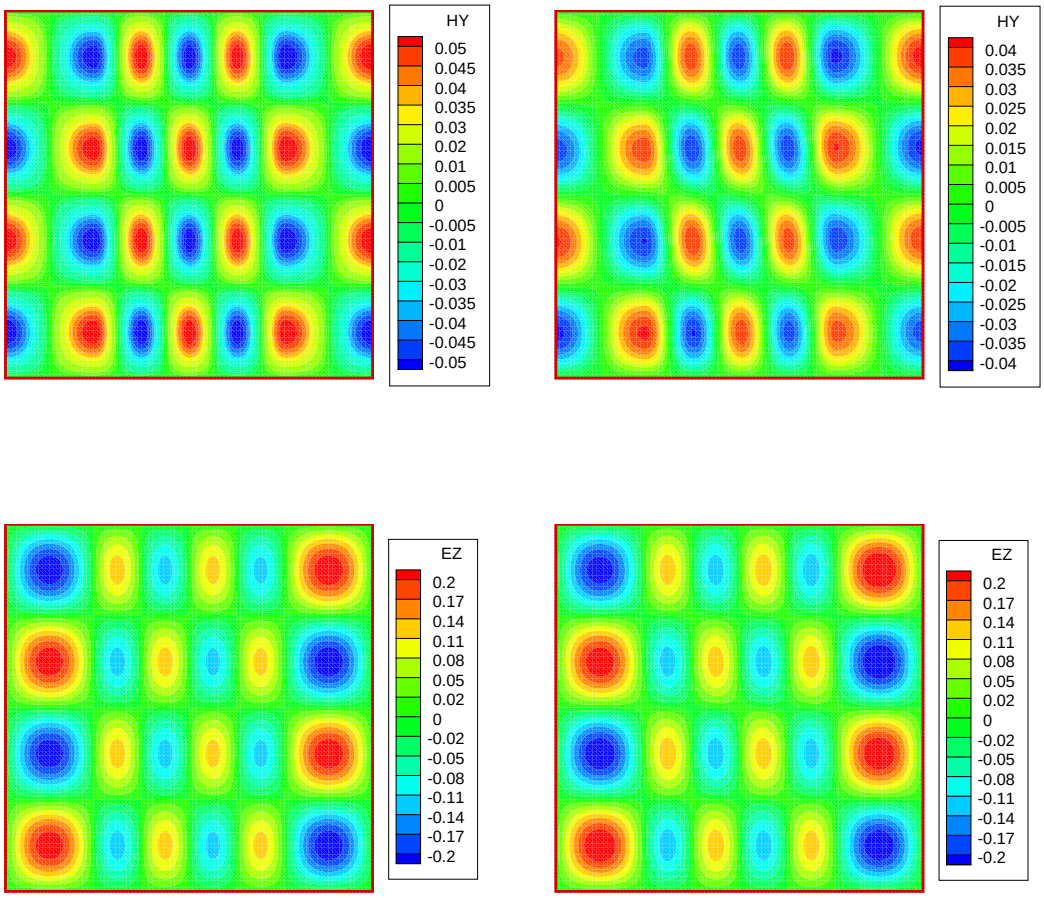

Figure 4.7: *Dielectric in a PEC cavity with two material interfaces. Contour lines of H_y (top) and E_z (bottom) at $t = 1$ (left) and $t = 10$ (right). DGTD-$\mathbb{P}_1$ method using a conforming mesh with* 10201 *nodes and* 20000 *triangles.*

Table 4.7: *Dielectric in a PEC cavity with two material interfaces. Relative permittivities for different materials.*

Material/medium	ϵ_r
Air	1.0
Teflon	2.1
Polyethylene	2.25
Polystyrene	2.6
Ice at 0°C	3.2
Pyrex	4.7

Table 4.8: *Dielectric in a PEC cavity with two material interfaces with $\epsilon_2 = 2.25$. Convergence study for the h-refinement DGTD-$\mathbb{P}_p$ method using conforming meshes. L^2 error, CPU time and # time steps are measured at $t = 0.65$.*

# DOF	error on E_z	convergence rate on E_z	error on H_y	convergence rate on H_y	error on (**E**,**H**)	convergence rate on (**E**,**H**)	CPU (s)	# time steps
				DGTD-$\mathbb{P}_0$				
4608	7.74E−03	–	2.05E−02	–	2.72E−02	–	1	23
18432	3.78E−03	1.03	1.01E−02	1.02	1.33E−02	1.03	4	45
73728	1.89E−03	1.00	4.60E−03	1.14	6.08E−03	1.13	29	89
294912	9.47E−04	1.00	1.78E−03	1.37	2.42E−03	1.33	224	177
				DGTD-$\mathbb{P}_1$				
9600	5.72E−03	–	1.38E−02	–	1.81E−02	–	< 2	62
38400	2.11E−03	1.44	4.85E−03	1.51	6.47E−03	1.48	12	123
153600	1.33E−03	0.67	2.79E−03	0.79	3.80E−03	0.77	96	246
614400	6.11E−04	1.12	1.27E−03	1.13	1.80E−03	1.08	770	491
				DGTD-$\mathbb{P}_2$				
19200	1.57E−03	–	1.51E−03	–	2.41E−03	–	4	92
76800	1.22E−03	0.36	1.22E−03	0.31	1.89E−03	0.35	29	184
307200	1.08E−03	0.17	1.08E−03	0.16	1.69E−03	0.16	244	368
1228800	6.58E−04	0.72	7.12E−04	0.61	1.08E−03	0.64	1936	736
				DGTD-$\mathbb{P}_3$				
32000	1.55E−03	–	1.44E−03	–	2.30E−03	–	13	184
128000	1.22E−03	0.35	1.21E−03	0.25	1.88E−03	0.29	104	368
512000	1.08E−03	0.17	1.08E−03	0.15	1.69E−03	0.15	875	736
2048000	6.58E−04	0.72	6.37E−04	0.77	1.00E−03	0.76	6817	1471

Table 4.9: *Dielectric in a PEC cavity with two material interfaces with $\epsilon_2 = 2.25$. Convergence study for the h-refinement DGTD-$\mathbb{P}_p$ method using non-conforming meshes. L^2 error, CPU time and # time steps are measured at $t = 0.65$.*

# DOF	error on E_z	convergence rate on E_z	error on H_y	convergence rate on H_y	error on (**E**,**H**)	convergence rate on (**E**,**H**)	CPU (s)	# time steps
				DGTD-$\mathbb{P}_0$				
2880	1.92E−02	–	2.38E−02	–	3.62E−02	–	< 1	23
11520	9.25E−03	1.06	1.25E−02	0.93	1.84E−02	0.98	2	45
46080	4.62E−03	1.00	6.08E−03	1.04	9.01E−03	1.03	18	89
184320	2.31E−03	1.00	2.73E−03	1.15	4.18E−03	1.11	142	177
				DGTD-$\mathbb{P}_1$				
8640	1.12E−02	–	1.48E−02	–	2.22E−02	–	< 2	74
34560	3.85E−03	1.54	6.49E−03	1.19	8.90E−03	1.32	13	148
138240	1.99E−03	0.95	3.00E−03	1.12	4.28E−03	1.06	105	295
552960	1.01E−03	0.98	1.50E−03	1.00	2.22E−03	0.95	824	589
				DGTD-$\mathbb{P}_2$				
48000	1.56E−03	–	1.46E−03	–	2.33E−03	–	18	184
192000	1.22E−03	0.36	1.28E−03	0.27	1.88E−03	0.31	148	368
768000	1.08E−03	0.17	1.08E−03	0.16	1.69E−03	0.15	1218	736
3072000	6.58E−04	0.72	7.11E−04	0.61	1.08E−03	0.65	10110	1472
				DGTD-$\mathbb{P}_3$				
80000	1.56E−03	–	1.44E−03	–	2.30E−03	–	65	368
320000	1.22E−03	0.35	1.20E−03	0.26	1.88E−03	0.30	596	736
1280000	1.08E−03	0.17	1.08E−03	0.16	1.69E−03	0.15	5487	1472
5120000	6.58E−04	0.72	6.39E−04	0.76	1.00E−03	0.75	51103	2944

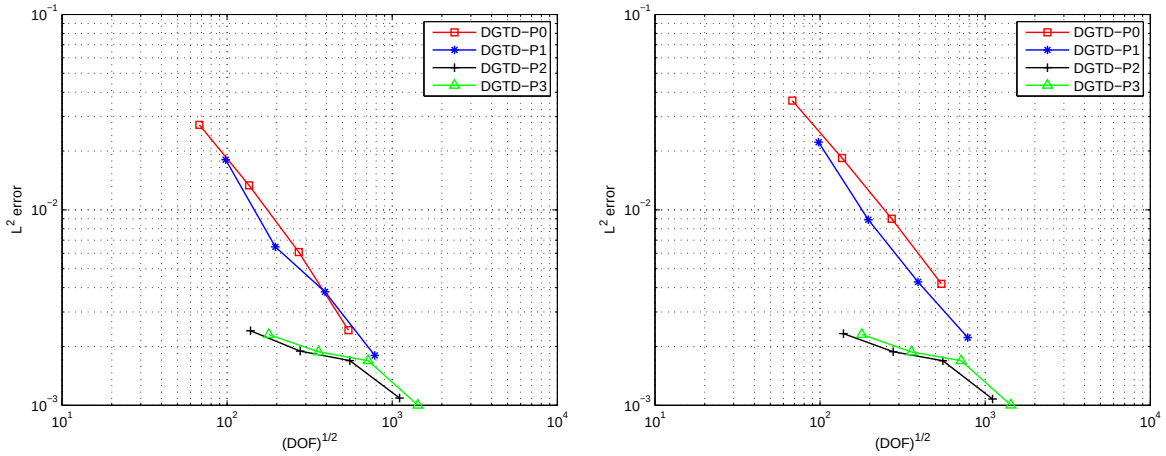

Figure 4.8: *Dielectric in a PEC cavity with two material interfaces with* $\epsilon_2 = 2.25$. *Numerical convergence of the h-refinement DGTD-*$\mathbb{P}_p$ *method. Conforming (left) and non-conforming (right) triangular meshes.*

Table 4.10: *Dielectric in a PEC cavity with two material interfaces with* $\epsilon_2 = 2.25$. *Convergence study of the DGTD-*$\mathbb{P}_{p_c}$:$\mathbb{P}_{p_f}$ *method. Non-conforming locally refined meshes.* L^2 *error, CPU time and # time steps are measured at* $t = 0.65$.

# DOF	error on E_z	convergence rate on E_z	error on H_y	convergence rate on H_y	error on (**E**,**H**)	convergence rate on (**E**,**H**)	CPU (s)	# time steps
				DGTD-$\mathbb{P}_1$:$\mathbb{P}_0$				
4032	1.49E−02	–	2.37E−02	–	3.31E−02	–	< 1	32
16128	6.34E−03	1.23	1.28E−02	0.88	1.72E−02	0.95	4	64
64512	3.46E−03	0.87	6.28E−03	1.03	8.46E−03	1.02	34	127
258048	1.87E−03	0.89	3.10E−03	1.02	4.21E−03	1.01	280	253
				DGTD-$\mathbb{P}_2$:$\mathbb{P}_0$				
5760	1.50E−02	–	1.83E−02	–	2.73E−02	–	1	56
23040	5.04E−03	1.57	7.79E−03	1.23	1.10E−02	1.31	8	111
92160	3.01E−03	0.74	4.25E−03	0.87	5.92E−03	0.89	69	221
368640	1.75E−03	0.78	2.46E−03	0.79	3.39E−03	0.81	498	442
				DGTD-$\mathbb{P}_2$:$\mathbb{P}_1$				
10368	1.32E−02	–	1.15E−02	–	1.93E−02	–	2	74
41472	3.29E−03	2.00	4.30E−03	1.42	5.54E−03	1.80	16	148
165888	1.77E−03	0.89	2.19E−03	0.97	3.01E−03	0.88	126	295
663552	9.37E−04	0.92	1.18E−03	0.89	1.75E−03	0.78	933	589
				DGTD-$\mathbb{P}_3$:$\mathbb{P}_1$				
12672	1.31E−02	–	1.19E−02	–	1.96E−02	–	3	89
50688	2.94E−03	2.16	2.92E−03	2.03	4.06E−03	2.27	21	177
202752	1.65E−03	0.83	1.63E−03	0.85	2.37E−03	0.78	175	353
811008	9.37E−04	0.82	1.06E−03	0.61	1.62E−03	0.55	1402	706
				DGTD-$\mathbb{P}_3$:$\mathbb{P}_2$				
54400	1.56E−03	–	1.44E−03	–	2.31E−03	–	21	184
217600	1.22E−03	0.35	1.21E−03	0.26	1.88E−03	0.30	172	368
870400	1.08E−03	0.17	1.08E−03	0.15	1.69E−03	0.15	1392	736
3481600	6.56E−04	0.72	7.02E−04	0.63	1.07E−03	0.66	11270	1472

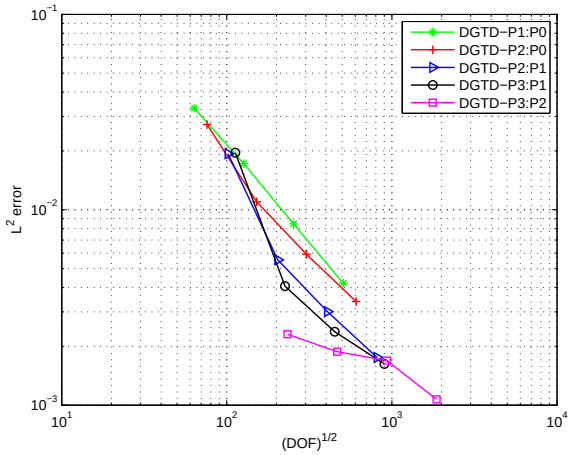

Figure 4.9: *Dielectric in a PEC cavity with two material interfaces with* $\epsilon_2 = 2.25$. *Numerical convergence of the hp-refinement DGTD-*$\mathbb{P}_{p_c}$*-*$\mathbb{P}_{p_f}$ *method. Non-conforming triangular meshes.*

Table 4.11: *Dielectric in a PEC cavity with two material interfaces for different types of materials. Convergence study of the DGTD-*$\mathbb{P}_p$ *method using conforming meshes. L^2 error, CPU time and # time steps are measured at* $t = 0.65$.

	$\epsilon_2 = 1.00$ $\omega = \sqrt{5}\pi$		$\epsilon_2 = 1.25$ $\omega = 6.574295470$		$\epsilon_2 = 2.10$ $\omega = 9.217644926$	
# DOF	error on E_z	convergence rate on E_z	error on E_z	convergence rate on E_z	error on E_z	convergence rate on E_z
	DGTD-$\mathbb{P}_0$		DGTD-$\mathbb{P}_0$		DGTD-$\mathbb{P}_0$	
3200	2.71E−02	–	1.74E−02	–	1.56E−02	–
12800	1.40E−02	0.95	9.15E−03	0.93	7.21E−03	1.11
51200	7.14E−03	0.97	4.69E−03	0.96	3.59E−03	1.01
204800	3.60E−03	0.99	2.38E−03	0.98	1.79E−03	1.00
	DGTD-$\mathbb{P}_1$		DGTD-$\mathbb{P}_1$		DGTD-$\mathbb{P}_1$	
9600	1.26E−02	–	2.14E−02	–	7.34E−03	–
38400	3.19E−03	1.98	1.16E−02	0.90	4.67E−03	0.65
153600	8.64E−04	1.89	6.10E−03	0.93	3.02E−03	0.63
614400	2.02E−04	2.10	3.14E−03	0.96	1.70E−03	0.83
	DGTD-$\mathbb{P}_2$		DGTD-$\mathbb{P}_2$		DGTD-$\mathbb{P}_2$	
19200	5.34E−04	–	2.47E−02	–	4.17E−03	–
76800	1.26E−04	2.09	1.26E−02	0.97	4.88E−03	−0.2
307200	3.14E−05	2.00	6.39E−03	0.99	3.13E−03	0.64
1228800	7.74E−06	2.02	3.21E−03	0.99	1.73E−03	0.85
	DGTD-$\mathbb{P}_3$		DGTD-$\mathbb{P}_3$		DGTD-$\mathbb{P}_3$	
32000	1.22E−04	–	2.49E−02	–	4.16E−03	–
128000	3.11E−05	1.97	1.27E−02	0.97	4.88E−03	−0.2
512000	7.63E−06	2.03	6.39E−03	0.99	3.13E−03	0.64
2048000	1.65E−06	2.21	3.21E−03	0.99	1.73E−03	0.85

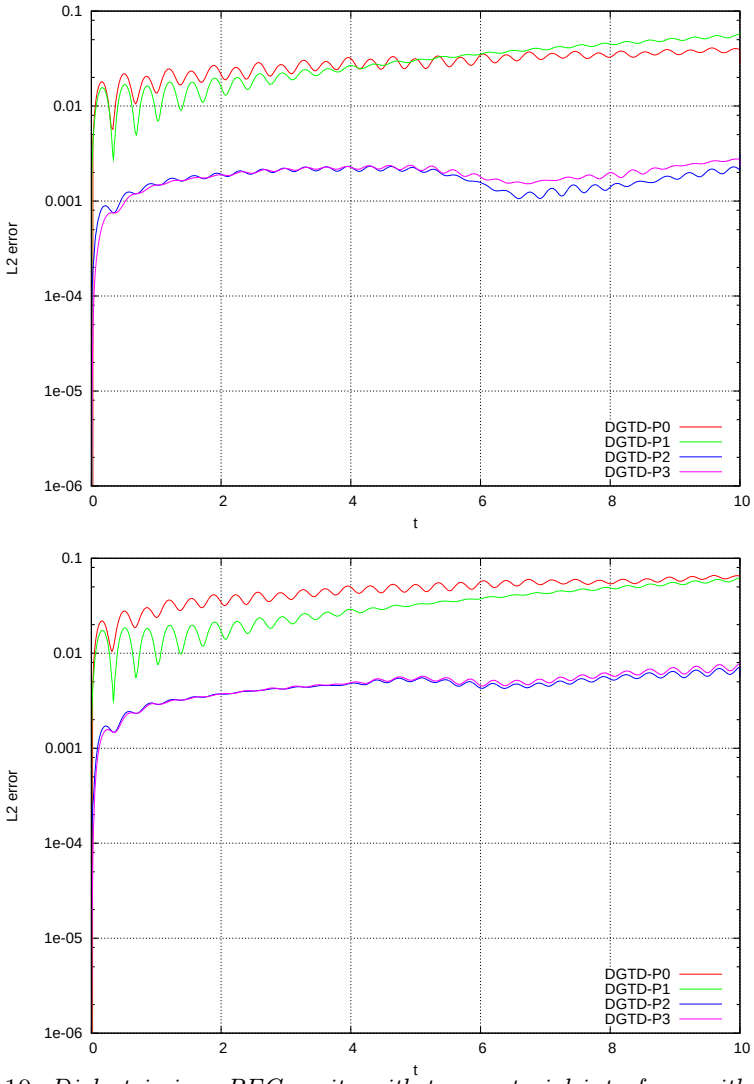

Figure 4.10: *Dielectric in a PEC cavity with two material interfaces with* $\epsilon_2 = 2.25$. *Time evolution of the* L^2 *error using the h-refinement DGTD-*$\mathbb{P}_p$ *method. Conforming (top) and non-conforming (bottom) triangular meshes.*

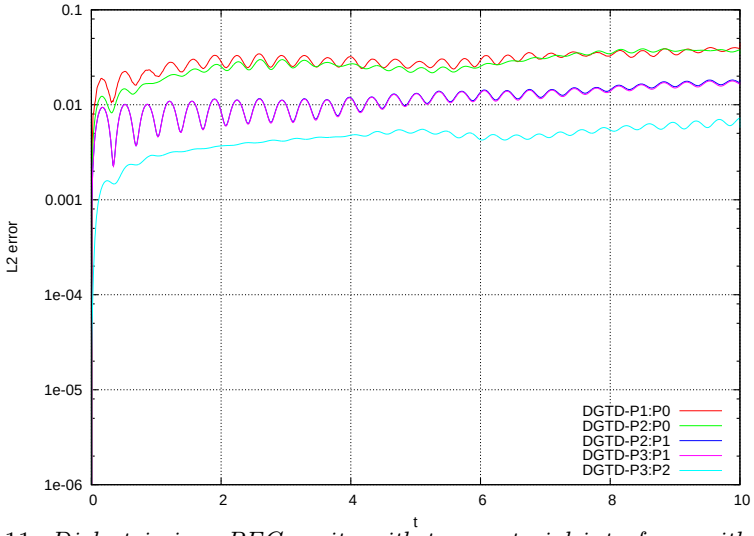

Figure 4.11: *Dielectric in a PEC cavity with two material interfaces with* $\epsilon_2 = 2.25$. *Time evolution of the* L^2 *error using the hp-refinement DGTD-*$\mathbb{P}_{p_c}$*:*$\mathbb{P}_{p_f}$ *method. Non-conforming triangular meshes.*

Table 4.12: *Dielectric in a PEC cavity with two material interfaces for different types of materials. Convergence study of the DGTD-*$\mathbb{P}_p$ *method using conforming meshes.* L^2 *error, CPU time and # time steps are measured at* $t = 0.65$.

# DOF	$\epsilon_2 = 2.60$, $\omega = 8.819946882$		$\epsilon_2 = 3.20$, $\omega = 6.480642472$		$\epsilon_2 = 4.70$, $\omega = 8.987555688$	
	error on E_z	convergence rate on E_z	error on E_z	convergence rate on E_z	error on E_z	convergence rate on E_z
	DGTD-$\mathbb{P}_0$		DGTD-$\mathbb{P}_0$		DGTD-$\mathbb{P}_0$	
3200	4.04E−03	–	3.67E−02	–	9.60E−03	–
12800	1.89E−03	1.10	1.73E−02	1.09	3.89E−03	1.30
51200	9.40E−04	1.01	8.50E−03	1.02	1.84E−03	1.07
204800	4.70E−04	1.00	4.24E−03	1.00	9.07E−04	1.02
	DGTD-$\mathbb{P}_1$		DGTD-$\mathbb{P}_1$		DGTD-$\mathbb{P}_1$	
9600	4.96E−03	–	1.04E−01	–	9.84E−03	–
38400	1.53E−03	1.69	5.75E−02	0.85	1.47E−03	2.74
153600	5.12E−04	1.58	3.01E−02	0.93	5.73E−04	1.36
614400	1.91E−04	1.43	1.54E−02	0.97	2.95E−04	0.96
	DGTD-$\mathbb{P}_2$		DGTD-$\mathbb{P}_2$		DGTD-$\mathbb{P}_2$	
19200	4.43E−03	–	1.11E−01	–	7.40E−03	–
76800	1.37E−03	1.69	5.96E−02	0.90	4.15E−04	4.16
307200	4.70E−04	1.54	3.07E−02	0.96	6.36E−04	−0.6
1228800	1.82E−04	1.37	1.55E−02	0.98	5.21E−04	0.29
	DGTD-$\mathbb{P}_3$		DGTD-$\mathbb{P}_3$		DGTD-$\mathbb{P}_3$	
32000	4.43E−03	–	1.11E−01	–	7.39E−03	–
128000	1.37E−03	1.69	5.96E−02	0.90	4.14E−04	4.16
512000	4.71E−04	1.54	3.07E−02	0.96	6.36E−04	−0.6
2048000	1.82E−04	1.37	1.56E−02	0.98	5.21E−04	0.29

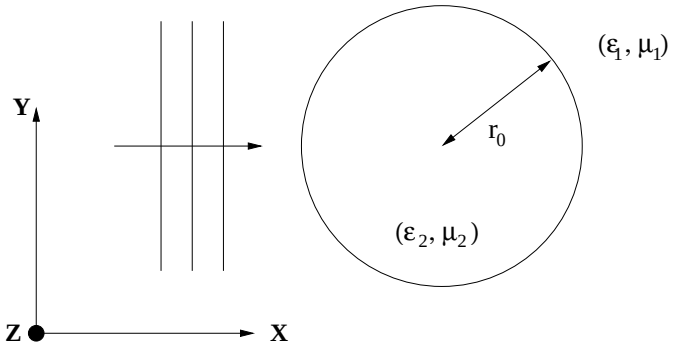

Figure 4.12: *Scattering of a dielectric cylinder setting.*

$$E_z^{\text{inc}} = \exp(-\mathsf{i}(k_1 x - \omega t)) \quad , \quad H_y^{\text{inc}} = -\exp(-\mathsf{i}(k_1 x - \omega t))$$

where $k_1 = \omega\sqrt{\epsilon_1\mu_1}$. In this case, the exact solution of the scattering problem is given by:

$$E_z(x,y,t) = E_z(r,\theta,t) = \exp(\mathsf{i}\omega t)\begin{cases} \displaystyle\sum_{n=-\infty}^{\infty} C_n^{\text{tot}} J_n(k_2 r)\exp(\mathsf{i}n\theta), & r \le r_0, \\ \displaystyle\sum_{n=-\infty}^{\infty} (\mathsf{i}^{-n} J_n(k_1 r) + C_n^{\text{scat}} H_n^{(2)}(k_1 r))\exp(\mathsf{i}n\theta), & r > r_0, \end{cases}$$

where J_n and $H_n^{(2)}$ represent the n-th order Bessel function of the first kind and the Hankel function of the second kind, respectively, and $k_2 = \omega\sqrt{\epsilon_2\mu_2}$ is the propagation constant for homogeneuous, lossless dielectric medium. As usual, $(r,\theta) = (\sqrt{x^2+y^2}, \arctan(y/x))$ represent the usual polar coordinates. The expansion coefficients for the total field interior to the cylinder are:

$$C_n^{\text{tot}} = \mathsf{i}^{-n}\frac{(k_1/\mu_1)J_n'(k_1 r_0)H_n^{(2)}(k_1 r_0) - (k_1/\mu_1)H_n^{(2)'}(k_1 r_0)J_n(k_1 r_0)}{(k_2/\mu_2)J_n'(k_2 r_0)H_n^{(2)}(k_1 r_0) - (k_1/\mu_1))H_n^{(2)'}(k_1 r_0)J_n(k_2 r_0)}.$$

The corresponding coefficients for the scattered field are:

$$C_n^{\text{scat}} = \mathsf{i}^{-n}\frac{(k_1/\mu_1)J_n'(k_1 r_0)J_n(k_2 r_0) - (k_2/\mu_2)J_n'(k_2 r_0)J_n(k_1 r_0)}{(k_2/\mu_2)J_n'(k_2 r_0)H_n^{(2)}(k_1 r_0) - (k_1/\mu_1)H_n^{(2)'}(k_1 r_0)J_n(k_2 r_0)}.$$

Using Maxwell's equations (2.1), one can recover the solutions for the magnetic field components. Then, the angular component of the total magnetic field is:

$$H_\theta(r,\theta,t) = -\exp(\mathsf{i}\omega t)\begin{cases} \dfrac{-\mathsf{i}k_2}{\omega\mu_2}\displaystyle\sum_{n=-\infty}^{\infty} C_n^{\text{tot}} J_n'(k_2 r)\exp(\mathsf{i}n\theta), & r \le r_0, \\ \dfrac{-\mathsf{i}k_1}{\omega\mu_1}\displaystyle\sum_{n=-\infty}^{\infty} (\mathsf{i}^{-n} J_n'(k_1 r) + C_n^{\text{scat}} H_n^{(2)'}(k_1 r))\exp(\mathsf{i}n\theta), & r > r_0, \end{cases}$$

and the radial component is:

$$H_r(r,\theta,t) = -\exp(\mathsf{i}\omega t)\begin{cases} \dfrac{\mathsf{i}}{\omega\mu_2 r}\displaystyle\sum_{n=-\infty}^{\infty} \mathsf{i}nC_n^{\text{tot}} J_n(k_2 r)\exp(\mathsf{i}n\theta), & r \le r_0, \\ \dfrac{\mathsf{i}}{\omega\mu_1 r}\displaystyle\sum_{n=-\infty}^{\infty} \mathsf{i}n(\mathsf{i}^{-n}J_n(k_1 r) + C_n^{\text{scat}} H_n^{(2)}(k_1 r))\exp(\mathsf{i}n\theta), & r > r_0. \end{cases}$$

Similarly to the previous test cases, we study the convergence of the DGTD-$\mathbb{P}_p$ and DGTD-$\mathbb{P}_{p_c}$:$\mathbb{P}_{p_f}$ methods for solving this scattering problem using conforming and non-conforming meshes. To this end, we consider a situation in which $\mu_1 = \mu_2 = \epsilon_1 = 1$, *i.e.* the material is non-magnetic, and the material exterior to the cylinder is assumed to be vacuum. The cylinder has a radius $r_0 = 0.6$ and bounds a material of relative permittivity $\epsilon_2 = 2.25$. The angular frequency is $\omega = 2\pi$ and the computational domain Ω is chosen as a cylinder of radius one, centered at $(0,0)$. In this special case, all three field components are continuous across the material interface. The first derivative of E_z is also continuous across the interface, but first derivatives of H_x and H_y are discontinuous. Regarding the boundary condition at the artificial boundary of the computational domain, we use a first order Silver-Müller absorbing boundary condition. Contour lines of the E_z and H_y components at times $t = 1$ and $t = 10$ are shown on Fig. 4.13 for a calculation based on the conforming DGTD-$\mathbb{P}_1$ method.

This problem has been studied in [33] in a scattered field/total field formulation using a FDTD method, and in [20]-[17]-[32] using a pseudospectral time-domain method with a stabilized PML absorbing boundary condition. It is also solved in [6] using a central finite difference scheme away from the material interfaces and upwinding technique with jump conditions near the interfaces and exact boundary conditions. Cai et al [23] developed a discontinuous Galerkin method for this problem. This method combined upwinding fluxes with a Runge-Kutta time scheme and the fields are approximated using Legendre polynomials for rectangular elements and standard nodal polynomials for triangular elements. Recently, Deng and Cai [11] propose an extension of [23] to a higher order method based on orthogonal non-polynomial nodal basis on triangles.

***h*-refinement DGTD-$\mathbb{P}_p$ method.** We first construct three conforming meshes whose characteristics are summarized in Tab. 4.13. Then, non-conforming meshes are obtained by locally refining (one refinement level) the dielectric region of the conforming meshes. The characteristics of the resulting non-conforming meshes are summarized in Tab. 4.14. Tab. 4.15 and 4.16 give the L^2 error on $(\mathbf{E},\mathbf{H})$, the convergence rate, the CPU time and the number of time steps to reach $t = 1$ using conforming and non-conforming meshes. Fig. 4.14 shows the corresponding L^2 error on $(\mathbf{E},\mathbf{H})$ as a function of the square root of the number of DOF. It can be deduced from Tab. 4.15 and 4.16 that the convergence rate of the DGTD-$\mathbb{P}_p$ method is close to $\mathcal{O}(h^{(1)})$ for $p = 0, 1$, and very slow for $p = 2, 3$. It is clear also that it is not necessary to increase the interpolation degree to more than 1, since the convergence rate is not improved and this results in increased CPU time and memory usage.

Table 4.13: *Scattering of a dielectric cylinder. Characteristics of the three conforming meshes.*

	# nodes	# triangles
mesh-C1	101	190
mesh-C2	401	780
mesh-C3	1601	3160

***hp*-refinement DGTD-$\mathbb{P}_{p_c}$:$\mathbb{P}_{p_f}$ method.** We still make use of the non-conforming meshes given in Tab. 4.14. Tab. 4.17 gives the L^2 error on $(\mathbf{E},\mathbf{H})$, the convergence rate, the CPU time and the number

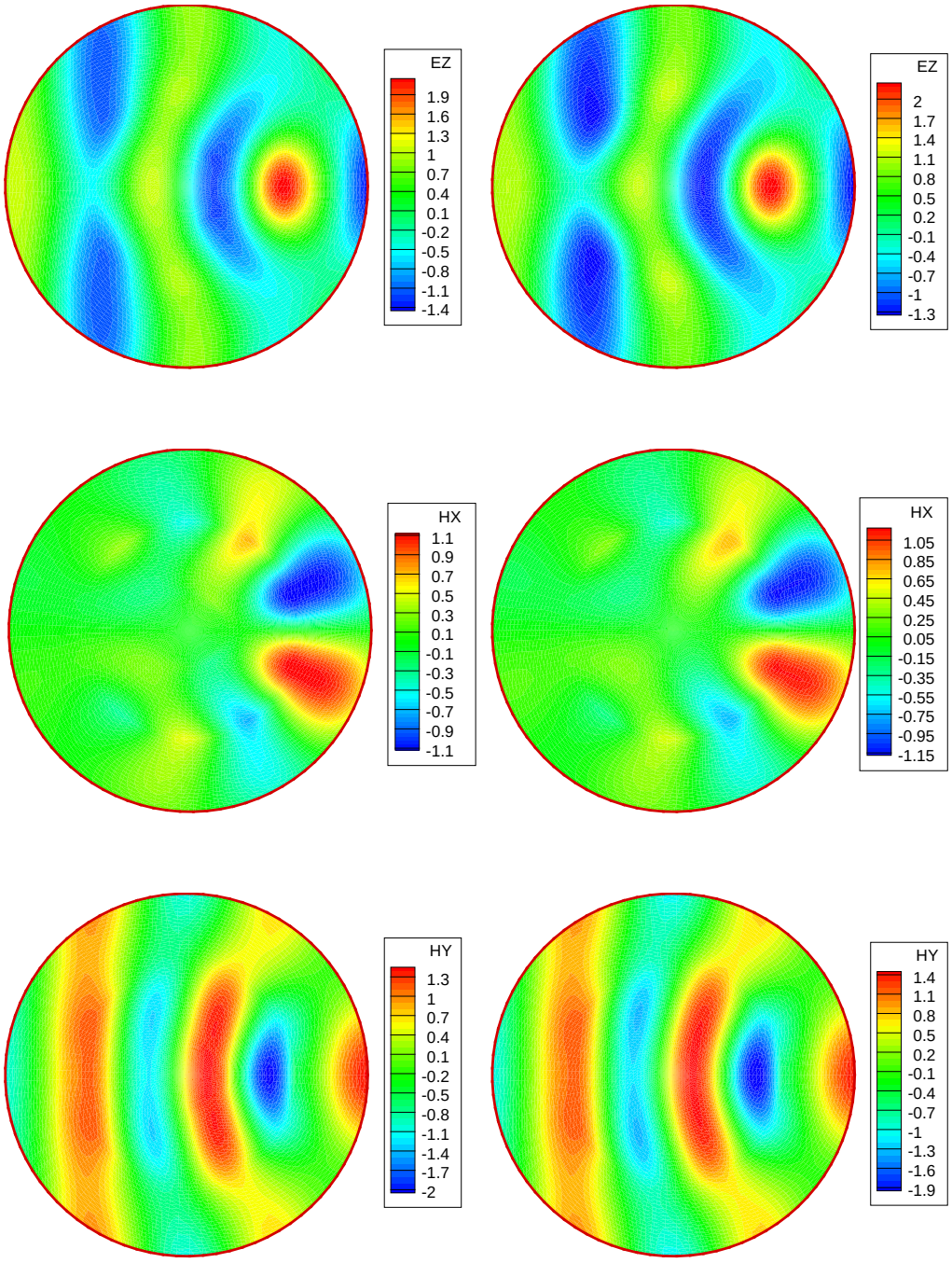

Figure 4.13: *Scattering of a dielectric cylinder.*
Contour lines of E_z (top), H_x (middle) and H_y (bottom) at $t = 1$ (left) and $t = 10$ (right).
DGTD-$\mathbb{P}_1$ method using a conforming mesh with 4251 *nodes and* 8415 *triangles.*

Table 4.14: *Scattering of a dielectric cylinder. Characteristics of the three non-conforming meshes.*

	# total nodes	# fine triangles	# coarse triangles	# hanging nodes
mesh-NC1	261	400	90	20
mesh-NC2	1021	1600	380	40
mesh-NC3	4041	6400	1560	80

Table 4.15: *Scattering of a dielectric cylinder. Convergence study for the h-refinement DGTD-$\mathbb{P}_p$ method using conforming meshes. L^2 error, CPU time and # time steps are measured at $t = 1$.*

# DOF	error of (**E**,**H**)	convergence rate on (**E**,**H**)	CPU (s)	# time steps
		DGTD-$\mathbb{P}_0$		
190	1.45E−00	–	< 1	23
780	6.43E−01	1.15	4	71
3160	3.22E−01	0.99	44	262
		DGTD-$\mathbb{P}_1$		
570	9.39E−01	–	4	76
2340	3.84E−01	1.26	30	236
9480	1.86E−01	1.03	427	874
		DGTD-$\mathbb{P}_2$		
1140	3.47E−01	–	7	113
4680	1.62E−01	1.07	85	354
18960	1.51E−01	0.11	1272	1310
		DGTD-$\mathbb{P}_3$		
1900	2.64E−01	–	23	226
7800	1.60E−01	0.70	283	708
31600	1.51E−01	0.09	4239	2620

Table 4.16: *Scattering of a dielectric cylinder. Convergence study for the h-refinement DGTD-$\mathbb{P}_p$ method using non-conforming meshes. L^2 error, CPU time and # time steps are measured at $t = 1$.*

# DOF	error of (**E**,**H**)	convergence rate on (**E**,**H**)	CPU (s)	# time steps
		DGTD-$\mathbb{P}_0$		
490	1.22E−00	–	2	46
1980	5.71E−01	1.09	7	82
7960	3.05E−01	0.90	88	262
		DGTD-$\mathbb{P}_1$		
1470	8.77E−01	–	9	151
5940	3.25E−01	1.42	65	272
23880	1.73E−01	0.90	845	874
		DGTD-$\mathbb{P}_2$		
2940	3.23E−01	–	27	226
11880	1.62E−01	0.99	193	408
47760	1.51E−01	0.10	2506	1310
		DGTD-$\mathbb{P}_3$		
4900	2.61E−01	–	87	452
19800	1.61E−01	0.70	633	816
79600	1.51E−01	0.09	8264	2620

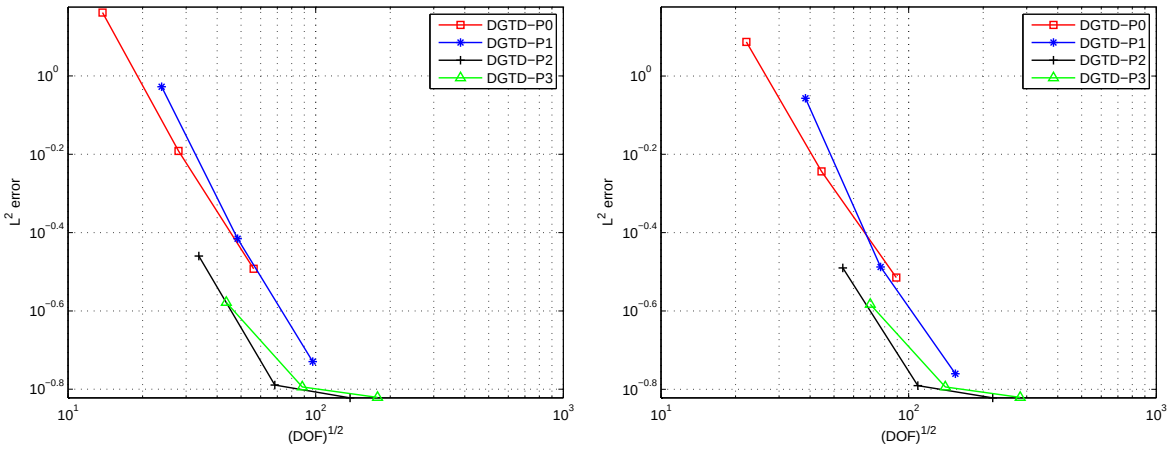

Figure 4.14: *Scattering of a dielectric cylinder.*
Numerical convergence of the h-refinement DGTD-$\mathbb{P}_p$ method.
Conforming (left) and non-conforming (right) triangular meshes.

of time steps to reach $t = 1$. Fig. 4.15 shows the corresponding L^2 error on $(\mathbf{E}, \mathbf{H})$ as a function of the square root of the number of DOF. It can be seen from Tab. 4.17 that the overall convergence rate of the DGTD-$\mathbb{P}_{p_c}$:$\mathbb{P}_{p_f}$ method is less than linear excepted for the DGTD-$\mathbb{P}_1$:$\mathbb{P}_0$ where the convergence rate is close to $\mathcal{O}(h^{(1)})$.

Table 4.17: *Scattering of a dielectric cylinder.*
Convergence study of the DGTD-$\mathbb{P}_{p_c}$:$\mathbb{P}_{p_f}$ method using non-conforming meshes.
L^2 error, CPU time and # time steps are measured at $t = 1$.

# DOF	error of (**E**,**H**)	convergence rate on (**E**,**H**)	CPU (s)	# time steps
		DGTD-$\mathbb{P}_1$:$\mathbb{P}_0$		
670	7.58E−01	–	5	113
2740	3.17E−01	1.23	28	204
11080	1.88E−01	0.75	363	655
		DGTD-$\mathbb{P}_2$:$\mathbb{P}_1$		
940	4.82E−01	–	13	226
3880	2.39E−01	0.99	89	408
15760	1.73E−01	0.46	1153	1310
		DGTD-$\mathbb{P}_2$:$\mathbb{P}_1$		
1740	4.16E−01	–	12	151
7080	1.78E−01	1.21	87	272
28560	1.51E−01	0.23	1134	874
		DGTD-$\mathbb{P}_3$:$\mathbb{P}_1$		
2100	3.66E−01	–	24	226
8600	1.76E−01	1.04	176	408
34800	1.52E−01	0.21	4566	2620
		DGTD-$\mathbb{P}_3$:$\mathbb{P}_2$		
3300	2.63E−01	–	33	226
13400	1.60E−01	0.71	239	408
54000	1.51E−01	0.08	6096	2620

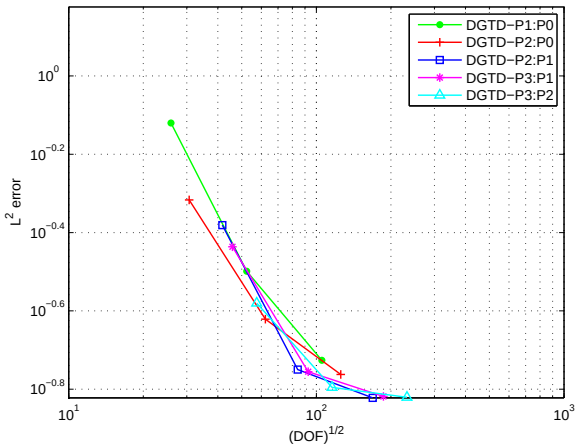

Figure 4.15: *Scattering of a dielectric cylinder.*
Numerical convergence of the hp-refinement DGTD-$\mathbb{P}_{p_c}$:$\mathbb{P}_{p_f}$ method.
Non-conforming triangular meshes.

5 Concluding remarks

In this work, we have presented the results of a detailed numerical evaluation of DGTD-$\mathbb{P}_p$ and DGTD-$\mathbb{P}_{p_c}$:$\mathbb{P}_{p_f}$ methods developed for the numerical solution of the two-dimensional time-domaine Maxwell equations on conforming and non-conforming triangular meshes. For this purpose, we have considered wave propagation problems in homogeneous and heterogeneous media. The DGTD-$\mathbb{P}_p$ and DGTD-$\mathbb{P}_{p_c}$:$\mathbb{P}_{p_f}$ methods were implemented in Fortran 77 and the computation was performed on a PC workstation equipped with an Intel Pentium M 1.7 GHz processor. The following conclusions can be drawn from these numerical experiments:

1. an optimal convergence rate is obtained for the DGTD-$\mathbb{P}_p$ ($p = 0, 1$) method in both homogeneous and heterogeneous media. For $p \geq 2$ the convergence rate is close to $\mathcal{O}(h^{(2)})$ in homogeneous case but it is linear or less in heterogeneous case.

2. the convergence rate of the DGTD-$\mathbb{P}_{p_c}$:$\mathbb{P}_{p_f}$ method for homogeneous media is close to $\mathcal{O}(h^{(2)})$, $\forall p_c$, $\forall p_f \neq 0$ and for $p_f = 0$ this convergence rate is close to $\mathcal{O}(h^{(3/2)})$. In heterogeneous media, the convergence rate of this method is linear or less, and in some particular cases we can obtain a convergence more than linear.

3. in homogeneous media, the DGTD-$\mathbb{P}_2$ and DGTD-$\mathbb{P}_2$:$\mathbb{P}_1$ methods are the most accurate and the least expensive *h*- and *hp*-refinement methods respectively. In heterogeneous media and to reach a given error level, the DGTD-$\mathbb{P}_0$ and DGTD-$\mathbb{P}_1$:$\mathbb{P}_0$ are the least expensive *h*- and *hp*-refinement methods. In general, the DGTD-$\mathbb{P}_{p_c}$:$\mathbb{P}_{p_f}$ method is less expensive than the DGTD-$\mathbb{P}_p$ method.

4. to obtain a high convergence rate for high order interpolation ($p \geq 2$), a high order time scheme like a fourth order leap-frog scheme must be used (see [25] for a 1D example). A special treatment of the numerical fluxes at material interfaces by using a regularization technique [2]-[22] may also improve the accuracy of the proposed method.

5. to reduce the costs of the method for a high order interpolation, three possible approaches can be used separately or in combination:

   - the use of hierarchical or orthogonal nodal basis functions can reduce the cost of memory consumption and can also improve the convergence rate of the *p*-enrichment method,

- the use of a local time stepping strategy [26],
- the use of an a posteriori error estimator which remains mandatory to reduce the costs of the method on non-conforming locally refined meshes.

Acknowledgment. The author would like to express his heartfelt gratitude to Stéphane Lanteri for many helpful discussions during the course of this work.

References

[1] S. Abarbanel, A. Ditkowski, and A. Yefet. Bounded error schemes for the wave equation on complex domains. Report 98-50, ICASE, 1998. NASA Langley Research Center, Hampton.

[2] U. Andersson. *Time-domain methods for the Maxwell equations.* PhD thesis, Royal Institute of Technologie, 2001.

[3] M. Bernacki, L. Fezoui, S. Lanteri, and S. Piperno. Parallel unstructured mesh solvers for heterogeneous wave propagation problems. *Appl. Math. Model.*, 30(8):744–763, 2006.

[4] A. Bossavit. Solving Maxwell equations in a closed cavity, and the question of spurious modes. *IEEE Trans. Magnetics*, 26:702–705, 1990.

[5] A. Buffa, P. Houston, and I. Perugia. Discontinuous Galerkin computation of the Maxwell eigenvalues on simplicial meshes. *J. Comput. Appl. Math.*, 204:317–333, 2007.

[6] W. Cai and S. Deng. An upwinding embedded boundary method for Maxwell's equations in media with material interfaces: 2D case. *J. Comput. Phys.*, 190:159–183, 2003.

[7] N. Canouet, L. Fezoui, and S. Piperno. Discontinuous Galerkin time-domain solution of Maxwell's equations on locally-refined nonconforming cartesian grids. *COMPEL*, 24(4):1381–1401, 2005.

[8] B. Cockburn, G.E. Karniadakis, and C.W. Shu, editors. *Discontinuous Galerkin methods. Theory, computation and applications*, volume 11 of *Lecture Notes in Computational Science and Engineering.* Springer-Verlag, 2000.

[9] G. Cohen, X. Ferrieres, and S. Pernet. A spatial high spatial order hexahedral discontinuous Galerkin method to solve Maxwell's equations in time domain. *J. Comp. Phys.*, 217(2):340–363, 2006.

[10] F. Collino, T. Fouquet, and P. Joly. Conservative space-time mesh refinement methods for the FDTD solution of Maxwell's equations. *J. Comp. Phys.*, 211(1):9–35, 2006.

[11] S. Deng and W. Cai. Analysis and application of an orthogonal nodal basis on triangles for discontinuous spectral element methods. *Appl. Num. Anal. Comp. Math.*, 2(3):326–345, 2005.

[12] A. Ditkowski, K. Dridi, and J.S. Hesthaven. Convergent cartesian grid methods for Maxwell's equations in complex geometries. *J. Comput. Phys.*, 170:39–80, 2001.

[13] K. Dridi, J. S. Hesthaven, and A. Ditkowski. Staircase-free finite-difference time-domain formulation for general materials in complex geometries. *IEEE Trans. Antennas Propag.*, 49:749–755, 2001.

[14] M. Duruflé. *Intégration numérique et éléments finis d'ordre élevé appliqués aux équations de Maxwell en régime harmonique.* PhD thesis, Université Paris Dauphine, 2006.

[15] H. Fahs, S. Lanteri, and F. Rapetti. Etude de stabilité d'une méthode Galerkin discontinu pour la résolution numérique des équations de Maxwell 2D en domaine temporel sur des maillages triangulaires non-conformes. Research Report 6023, INRIA, Juillet 2006.

[16] H. Fahs, S. Lanteri, and F. Rapetti. A *hp*-like discontinuous Galerkin method for solving the 2D time-domain Maxwell's equations on non-conforming locally refined triangular meshes. Research Report 6162, INRIA, 2007.

[17] G. X. Fan, Q. H. Liu, and J. S. Hesthaven. Multi-domain pseudospectral time-domain simulations of scattering by objects buried in lossy media. *IEEE Trans. Geosci. Remote Sens.*, 40(6):1366–1373, 2002.

[18] L. Fezoui, S. Lanteri, S. Lohrengel, and S. Piperno. Convergence and stability of a discontinuous Galerkin time-domain method for the heterogeneous Maxwell equations on unstructured meshes. *ESAIM: Math. Model. and Numer. Anal.*, 39(6):1149–1176, 2006.

[19] J. S. Hesthaven. High-order accurate methods in time-domain computational electromagnetics. *Adv. Imaging Elec. Phys.*, 127:59–123, 2003.

[20] J.S. Hesthaven, P. G. Dinesen, and J. P. Lynov. Spectral collocation time-domain modeling of diffractive optical elements. *J. Comput. Phys.*, 155(2):287–306, 1999.

[21] J.S. Hesthaven and T. Warburton. High-order nodal discontinuous Galerkin methods for the Maxwell's eigenvalue problem. *Royal Soc. London Ser. A*, 362:493–524, 2004.

[22] E. Kashdan. *High-order accurate methods for Maxwell equations*. PhD thesis, Tel Aviv University, 2004.

[23] T. Lu, P. Zhang, and W. Cai. Discontinuous Galerkin methods for dispersive and lossy Maxwell's equations and PML boundary conditions. *J. Comput. Phys.*, 200:549–580, 2004.

[24] J. C. Nedelec. A new family of mixed finite elements in $\mathbb{R}^3$. *Numer. Math.*, 50:57–81, 1986.

[25] S. Piperno. Schémas en éléments finis discontinus localement raffinés en espace et en temps pour les équations de Maxwell 1D. Research Report 4986, INRIA, 2003.

[26] S. Piperno. Simplectic local time-stepping in non-dissipative DGTD methods applied to wave propagation problems. *M2AN*, 40(5):815–841, 2006.

[27] A.C. Polycarpou, C.A. Balanis, and A. Stefanov. Helicopter rotor-blade modulation of antenna radiation characteristics. *IEEE Trans. Antennas Propagat.*, 49:688–696, 2001.

[28] W. Rachowicz and A. Zdunek. An *hp*-adaptive finite element method for scattering problems in computational electromagnetics. *Int. J. Numer. Engng.*, 62:1226–1249, 2005.

[29] F. Reitich and K.K. Tamma. State-of-the-art, trends and directions in computational electromagnetics. *Comput. Meth. Eng. Sci.*, 5:287–294, 2004.

[30] J.-F. Remacle, J. Flaherty, and M. Shephard. An adaptive discontinuous Galerkin technique with an orthogonal basis applied to compressible flow problems. *SIAM Review*, 45(1):53–72, 2003.

[31] G. Scarella, O. Clatz, S. Lanteri, G. Beaume, S. Oudot, J.-P. Pons, S. Piperno, P. Joly, and J. Wiart. Realistic numerical modelling of human head tissue exposure to electromagnetic waves from cellular phones. *Comptes Rendus Physique*, 7(5):501–508, 2006.

[32] Y. Shi, L. Li, and C.-H. Liang. Two dimensional multidomain pseudospectral time-domain algorithm based on alternating-direction implicit method. *IEEE Trans. Antennas Propagat.*, 54(4):1207–1214, 2006.

[33] A. Taflove. *Advances in computational electrodynamics, the finite-difference time-domain method*. Artech House, Boston, London, 1998.

[34] A.-K. Tornberg and B. Engquist. Regularization techniques for numerical approximation of PDEs with singularities. *J. Sci. Comput.*, 19:527–552, 2003.

[35] E. Turkel and A. Yefet. Fourth order compact implicit method for the Maxwell equations with discontinuous coefficients. *Appl. Numer. Math.*, 33(1-4):125–134, 2000.

[36] E. Turkel and A. Yefet. On the construction of a high order difference scheme for complex domains in a cartesian grid. *Appl. Numer. Math.*, 33(1-4):113–124, 2000.

[37] T. Xiao and Q.H. Liu. A staggered upwind embedded boundary (SUEB) method to eliminate the FDTD staircasing error. *IEEE Trans. Antennas and Propagat.*, 52(3):730–741, 2004.

[38] Z. Xie, C.-H. Chan, and B. Zhang. An explicit fourth-order orthogonal curvilinear staggered-grid FDTD method for Maxwell's equations. *J. Comput. Phys.*, 175:739–763, 2002.

[39] K.S. Yee. Numerical solution of initial boundary value problems involving Maxwell's equations in isotropic media. *IEEE Trans. Antennas and Propagat.*, 14(3):302–307, 1966.

[40] A. Yefet and P. G. Petropoulos. A staggered fourth-order accurate explicit finite difference scheme for the time-domain Maxwell's equations. *J. Comp. Phys.*, 168(2):286–315, 2001.

[41] S. Zhao and G. W. Wei. High-order FDTD methods via derivative matching for Maxwell's equations with material interfaces. *J. Comp. Phys.*, 200(1):60–103, 2004.

Unité de recherche INRIA Sophia Antipolis
2004, route des Lucioles - BP 93 - 06902 Sophia Antipolis Cedex (France)

Unité de recherche INRIA Futurs : Parc Club Orsay Université - ZAC des Vignes
4, rue Jacques Monod - 91893 ORSAY Cedex (France)
Unité de recherche INRIA Lorraine : LORIA, Technopôle de Nancy-Brabois - Campus scientifique
615, rue du Jardin Botanique - BP 101 - 54602 Villers-lès-Nancy Cedex (France)
Unité de recherche INRIA Rennes : IRISA, Campus universitaire de Beaulieu - 35042 Rennes Cedex (France)
Unité de recherche INRIA Rhône-Alpes : 655, avenue de l'Europe - 38334 Montbonnot Saint-Ismier (France)
Unité de recherche INRIA Rocquencourt : Domaine de Voluceau - Rocquencourt - BP 105 - 78153 Le Chesnay Cedex (France)

Éditeur
INRIA - Domaine de Voluceau - Rocquencourt, BP 105 - 78153 Le Chesnay Cedex (France)
http://www.inria.fr
ISSN 0249-6399